Marine Geology 285 (2011) 29–45

Contents lists available at ScienceDirect

Marine Geology

journal homepage: www.elsevier.com/locate/margeo

Frontal emplacement and mobility of sublacustrine landslides: Results from morphometric and seismostratigraphic analysis

J. Moernaut *, M. De Batist

Renard Centre of Marine Geology, Ghent University, Krijgslaan 281 (S8), Ghent, Belgium

ARTICLE INFO

Article history:
Received 20 December 2010
Received in revised form 29 April 2011
Accepted 4 May 2011
Available online 11 May 2011

Communicated by D.J.W. Piper

Keywords:
sublacustrine landslides
morphometric analysis
frontal emplacement
reflection seismics

ABSTRACT

The morphometric characteristics of 96 sublacustrine landslide complexes were measured on dense grids of high-resolution seismic reflection data from several lakes worldwide and were statistically analyzed. This analysis reveals that the morphology of the sublacustrine slopes exerts a strong control on the size of slope failures that occur on them, as the location of the headscarp and frontal ramp of these landslides are mainly determined by changes in the slope gradient. Our dataset also shows that the height drop of the failing slope section and the subsurface depth of the basal shear surface are the main parameters that determine whether a landslide will propagate in a frontally confined or frontally emergent manner. These parameters respectively represent the gravitational potential energy (driving force) of the sliding mass and the potential energy required (a resisting force) for it to emerge at its frontal ramp. These observations open perspectives for predicting the frontal emplacement style of future sublacustrine and submarine landslides and their associated natural hazards (e.g., tsunamis, dense flows). Although the investigated sublacustrine landslides have smaller dimensions than most submarine landslides, our data reveal mostly comparable inter-parameter correlations and relationships. However, frontally emergent landslides in lakes (and fjords) generally have a larger mobility and underwent a larger disintegration than what would have been expected by extrapolation of empirical relationships derived for ocean margin landslide datasets. This can be explained by the highly-unconsolidated material usually involved in the shallowly excavated slope failures in lakes and fjords.

1. Introduction

Sublacustrine landslide deposits and their associated turbidites are important components of the sedimentary infill of many lakes and are increasingly used as proxy for past earthquake activity (e.g., Karlin et al., 2004; Strasser et al., 2006; Moernaut et al., 2007). Most of what is known today about subaqueous landslide processes has been obtained through a vast number of marine studies and modeling (e.g., Canals et al., 2004; Masson et al., 2006 and references therein). The use of 3D seismic datasets has allowed imaging and mapping of large-scale landslide complexes with unprecedented, data coverage and detail, and has helped revealing various types of kinematic indicators of mass-transport (Gee et al., 2005; Bull et al., 2009). For example, impressive fold-and-thrust systems in a landslide toe region were analyzed by Frey-Martinez et al. (2006) and allowed the construction of a 2-end-member model for the frontal emplacement style of submarine landslides (Fig. 1). This includes i) frontally confined landslides, in which the frontal part is buttressed against undisturbed slope strata, and ii) frontally emergent landslides, which are able to ramp up from their original stratigraphic position and translate in an unconfined way over the sea bottom. Frontally confined landslides are now beginning to be reported worldwide (e.g., Gafeira et al., 2007; Callot et al., 2008; Tripsanas et al., 2008; Lawrence and Cartwright, 2009; Gamberi et al., 2011), although the mechanisms and kinematics involved in their frontal emplacement are still poorly understood. For example, it has not yet been conclusively established why some submarine landslides stay confined while others do not, and if these different frontal behaviors produce dissimilar associated hazards (e.g., tsunami and high-velocity flows).

Hampton et al. (1996) compiled morphometric data of several submarine landslides known at that time and pointed out that they generally exhibit a larger mobility than subaerial landslides. Driven by advances in marine observation techniques, a vast amount of submarine landslide complexes have been discovered since then, which has allowed their morphometric parameters to be analyzed statistically (McAdoo et al., 2000; Hühnerbach et al., 2004; Green and Uken, 2008). Strong correlations were found between several area- and volume-related parameters, which can help in estimating the expected volume (and associated hazards) of a landslide given the subsurface depth of a potential failure plane. Sublacustrine landslides are on average smaller than submarine ones, but a comprehensive

* Corresponding author.
E-mail address: jasper.moernaut@ugent.be (J. Moernaut).

0025-3227/$ – see front matter © 2011 Elsevier B.V. All rights reserved.
doi:10.1016/j.margeo.2011.05.001

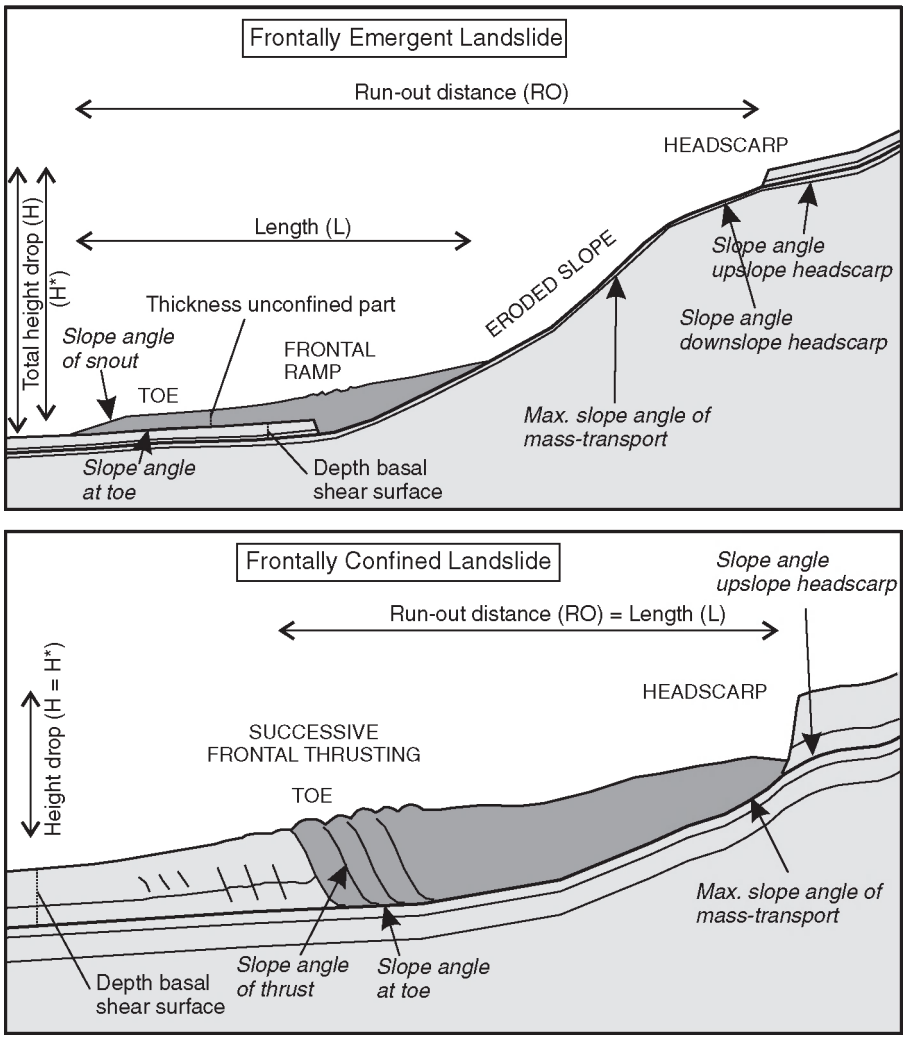

Fig. 1. Schematic illustration of frontally emergent and confined landslides with indication of the various morphometric parameters that were measured in this study. Note the difference between total height drop H (between headscarp and toe) and height drop H* (between headscarp and frontal ramp). Dark gray: landslide deposit (deformed and/or displaced sediment sequences); light gray: unfailed sediment sequences (with possible in-situ deformations/fractures near the landslide toe).

morphometric study of sublacustrine landslides has not yet been performed. Therefore, it is not known yet whether similar relationships exist and thus whether similar processes control the dimensions and geometry of sublacustrine landslides.

The aim of our study is therefore two-fold:

i) establishing which parameters determine whether a landslide develops a confined or emergent frontal emplacement style (in lacustrine environments);
ii) establishing the relationships between the morphometric parameters of sublacustrine landslides and their position with respect to submarine landslides.

Our study is based on the seismostratigraphic and morphometric analysis of sublacustrine landslides imaged on high to very-high resolution seismic-reflection data from lakes of various sizes and from various environments. We first present two selected case studies in order to illustrate the different features related to the frontal emplacement style of sublacustrine landslides. In the second part of the paper, we present the statistical analysis of the morphometric parameters of our landslide catalog. This combined approach allows testing the applicability of the hypotheses made in a particular case study on a broader scale.

2. Methods

Over the past 15 years, the Renard Centre of Marine Geology (RCMG; Ghent University) has collected high and very-high resolution seismic-reflection data in the framework of several national and international lake research projects (SI Table 1). These data were acquired using different acoustic sources, such as sparkers, boomers and pingers (SI Table 2), which were towed behind a GPS-positioned survey vessel. All seismic data were digitally recorded on a TRITON–ELICS Delph-2 acquisition system. Depending on data quality and user needs, post-acquisition data processing – including bandpass filtering, scaling and deconvolution – was carried out on a LANDMARK ProMax system. Seismostratigraphic interpretation was performed using Seismic Micro-Technology's Kingdom Suite package (version 7.5). An acoustic velocity of 1500 m/s was used for time-to-depth conversions in the water column and the upper sediments, which is in agreement with acoustic velocities derived from lacustrine refraction seismic data (e.g., Finckh et al., 1984), core logging data (e.g., Waldmann et al., 2008) and multi-channel seismic-reflection data (e.g., Scholz et al., 2002).

In this paper, we will only use the general terms "landslides" and "landslide deposits" as i) seismic data on their own are not sufficient to establish the exact mass-transport process behind the imaged

landslide deposits (Tripsanas et al., 2008), ii) landslides can evolve from one type into another (Mulder and Alexander, 2001a) and iii) various static and dynamic classification schemes, subdivisions and terminologies exist (e.g., Nardin et al., 1979; Mulder and Cochonat, 1996; Mulder and Alexander, 2001a; Tripsanas et al., 2008). We cataloged landslide complexes that originated from translational failure of subaqueous sedimentary slope sequences, thereby excluding deposits resulting from rotational landslides, rock falls, debris avalanches and turbidity currents (e.g., Hampton et al., 1996; Normark et al., 2004; Schnellmann et al., 2006). The scar region of translational landslides can be easily discriminated by the presence of a clear slide scarp and a bedding-parallel sliding surface. Translational landslide deposits typically show a chaotic-to-transparent seismic facies and can have a lens-shaped intercalating geometry (e.g., Schnellmann et al., 2002). Of the 26 lakes examined, only 12 contained a useful landslide record with i) good seismic data quality, and ii) sufficiently dense seismic coverage of the landslide deposits and slide scar region (SI Table 1; SI Fig. 1). The shallower lakes

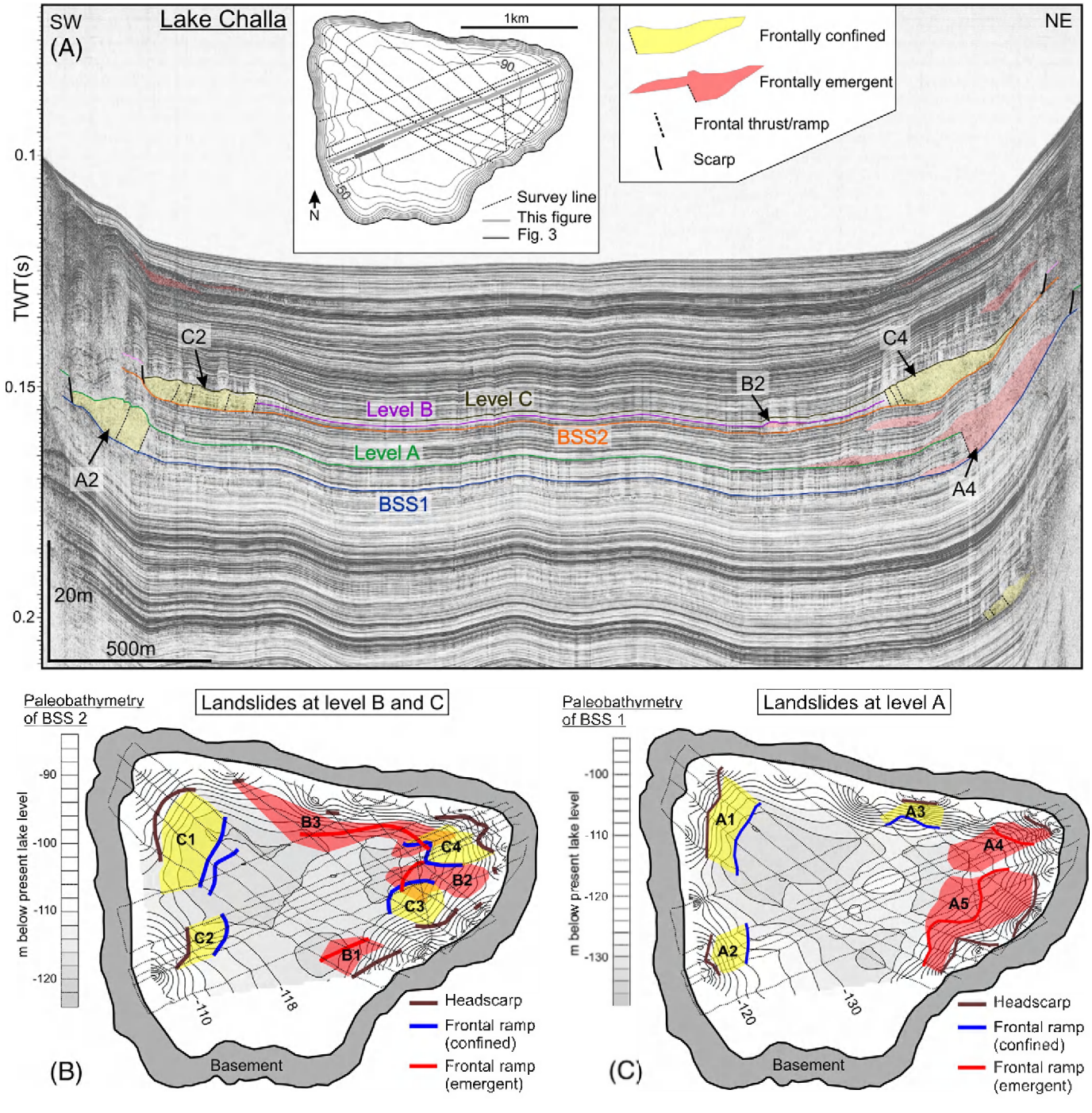

Fig. 2. A) Overview seismic profile of Lake Challa with landslide deposits at stratigraphic levels A, B and C. Two stratigraphic levels (BSS 1 and 2) were used as basal shear surface (BSS). Yellow: frontally confined landslides; Red: frontally emergent landslides. Inset figure at top: bathymetric map (isobaths every 10 m) and seismic survey lines. B) Paleobathymetric map of BSS 2 with level B and C landslides, which shared the same stratigraphic level as BSS (BSS 2). C) Paleobathymetric map of BSS 1 with level A landslides, which shared the same stratigraphic level as BSS (BSS 1).

(<~30 m water depth) do not contain any suitable landslide deposits, as the influence of wave action on the shallower lake bottom produces sediment focusing towards the deeper basin parts (Crusius and Anderson, 1995). This can prevent the build-up of sedimentary slope sequences prone to failure. Likewise, the fault-controlled lateral borders of the tectonic lakes in our database are often too steep for translational slope failure, as sediments generally do not accumulate in significant amounts on slopes steeper than about 14° (Håkanson and Jansson, 2002).

In this study, landslides are classified based on their frontal emplacement style as this characteristic can easily and objectively be determined on seismic-reflection profiles (Fig. 1). Frontally emergent landslides exhibit a larger downslope translation than frontally confined landslides, because the landslide has been able to ramp up from its original basal shear surface, abandon its scar surface and continue over the contemporaneous seafloor. On seismic sections, frontally confined landslides show frontal thrust structures in the toe region, separating uplifted, rotated and/or folded blocks of coherent strata from undeformed foreland sediments (e.g., Schnellmann et al., 2005). In downslope direction, buried frontally emergent landslides wedge out in between parallel-stratified reflections, which represent undisturbed units of pre- and postfailure sediments. Upslope, abrupt and steep transitions ("lateral margins") occur between the chaotic-to-transparent facies of the (confined and emergent) landslide deposits and the parallel-layered facies of the background sediments. For emergent landslides, a "frontal ramp" structure is located at the transition between the landslide scar and the main depositional area.

Up to 96 sublacustrine landslides fitting this two end-member model were identified and included in the database. Of these, 79 were classified as frontally emergent and 17 as frontally confined (SI Table 5). Dimensional measurements and slope calculations were carried out on seismic profiles and on maps to determine the morphometric parameters of the evacuational, translational and depositional area of each sublacustrine landslide, however with an emphasis on the depositional area (Fig. 1), where features are better visualized on the seismic data. The deposit volume was calculated using Golden Software SURFER software by subtracting the calculated grids for the landslide deposit bottom and top. This calculated deposit value might also provide a rough estimate of the failed sediment volume, assuming that only a minor fraction of the mass-movement transformed into turbidity currents. Several ratios between morphometric parameters were calculated and included in the statistical analysis.

3. Case study 1: Lake Challa

Lake Challa (4.2 km², 880 m a.s.l., maximum depth: 92 m) is a volcanic crater lake on the lower east slope of Mt. Kilimanjaro, on the border of Kenya and Tanzania. The sedimentary infill mostly has a uniform draping geometry, but detailed isopach mapping showed that certain seismic units display a partially basin-focused depositional pattern (Verschuren et al., 2009; Moernaut et al., 2010). Multiple landslide deposits were found at several stratigraphic levels (Fig. 2): e.g., A1–A5 at stratigraphic level A, B1–B3 at level B and C1–C4 at level C. The basal shear surfaces of level B and C landslides are located at a single stratigraphic level (BSS 2; Fig. 2). Level B landslides involved failure of a 0.7 m thick slope sequence, while this is 2.5 m thick for level C landslides. All landslides at level C are frontally confined, while these at the lower level B all show a frontally emergent geometry. Both types of landslides originated along the SE and E margin of the basin where slope profiles are quite similar to each other. The different emplacement style of level B and level C landslides suggests that the sub-surface depth of the basal shear surface (i.e., the thickness of the failed mass) plays an important role in controlling the ability of lacustrine slope failures to ramp out of their stratigraphic confinement (see Section 6).

On stratigraphic level A, two landslides are classified as frontally emergent while three landslides are frontally confined, but they all use the same stratigraphic level as basal shear surface (BSS 1). This indicates that factors other than the failed mass thickness control the frontal emplacement style. The values for the height drop between headscarp and frontal ramp (H^*) (9 m; 10 m) and maximum slope angle of mass-transport (1.9°; 2.5°) for confined landslides A1 and A2 are considerably lower than for the emergent landslides A4 and A5 (20 m and 22 m; 4.9° and 3.4°). Landslide A3 is not evaluated due to the scarcity and direction of seismic lines at this location. These results seem to indicate that the height drop H^* and slope angle could be primary parameters controlling the frontal emplacement style of sublacustrine landslides.

The seismic characteristics of an acoustically well-resolved frontally confined landslide (C2) were studied in high detail (Fig. 3). In the upslope region, a 2.6 m high headscarp is located on a downslope-steepening slope break (0° to 5°). This scarp is evidenced by a discontinuity in seismic reflections, diffraction hyperbola (in both directions) and more steeply dipping reflections above the scarp than beneath it. The landslide's basal shear surface is tied to one continuous reflector. The landslide deposit surface shows a smooth morphology in the upslope part and a rugged morphology in its toe region. A transition zone is located in between the chaotic-to-transparent facies of the landslide deposit and the horizontally laminated seismic facies of the undisturbed basin-plain sediments. This transition zone shows parallel reflections that correlate with the basin-plain units, but narrow, steeply west-ward dipping, low-amplitude zones disrupt the reflection continuity. In the most distal part, such acoustic wipe-out zones are restricted to the upper half of the transition zone and are more fragmented. The transition zone is considerably thicker (3.6 m thick) than the stratigraphically adjacent basin-plain unit (2.5 m thick). The rugged morphology at the toe of the confined landslide may be explained by the presence of a series of frontal thrusts (not visible on the profile) that developed where the foreland progressively failed under the gravitational downslope stress of the failing mass. These stresses also induced slope-parallel compression features (i.e., thickened unit, small fractures) in the transition zone, albeit without full failure of the sedimentary sequence. The confined-type frontal emplacement and the fact that the landslide deposit is located immediately at the foot of its headscarp indicate that only a limited downslope translation of the failed mass took place.

Thickness measurements for characterizing each confined landslide (Fig. 4) encompassed i) the undisturbed basin-plain sequence in front of the landslide, ii) the transition zone with compression features without full failure, and iii) the landslide's toe region where sediment packages are highly disturbed by frontal thrusting (failed zone). Compared to landslides at the same level, landslide A3 and C4 (Figs. 2 and4) exhibit the least thickening in the transition zone (107% and 129%), while having the most thickened toe region (180% and 221%). Conversely, landslides A1 and C1, which have the largest transition zone thickening (129% and 152%), exhibit relatively less failed zone thickening (167% and 184%). Furthermore, A3 and C4 exhibit higher values of height drop ($H = H^*$) and mean slope angle compared to landslides at the same level (Fig. 4). These results indicate that height drop and slope angle could be primary parameters in controlling the magnitude of frontal thrusting compared to thickening of the transition zone for confined landslides. Other parameters, such as the slope angle at toe or the length of the landslide did not correlate.

4. Case study 2: Lake le Bourget

Lake Le Bourget (18×2–3 km; 231 m a.s.l.; maximum depth: 145 m) is a glacigenic lake in the French NW Alps, the sedimentary infill of which has been extensively explored by means of high-resolution 2D seismics, side-scan sonar imaging, multibeam

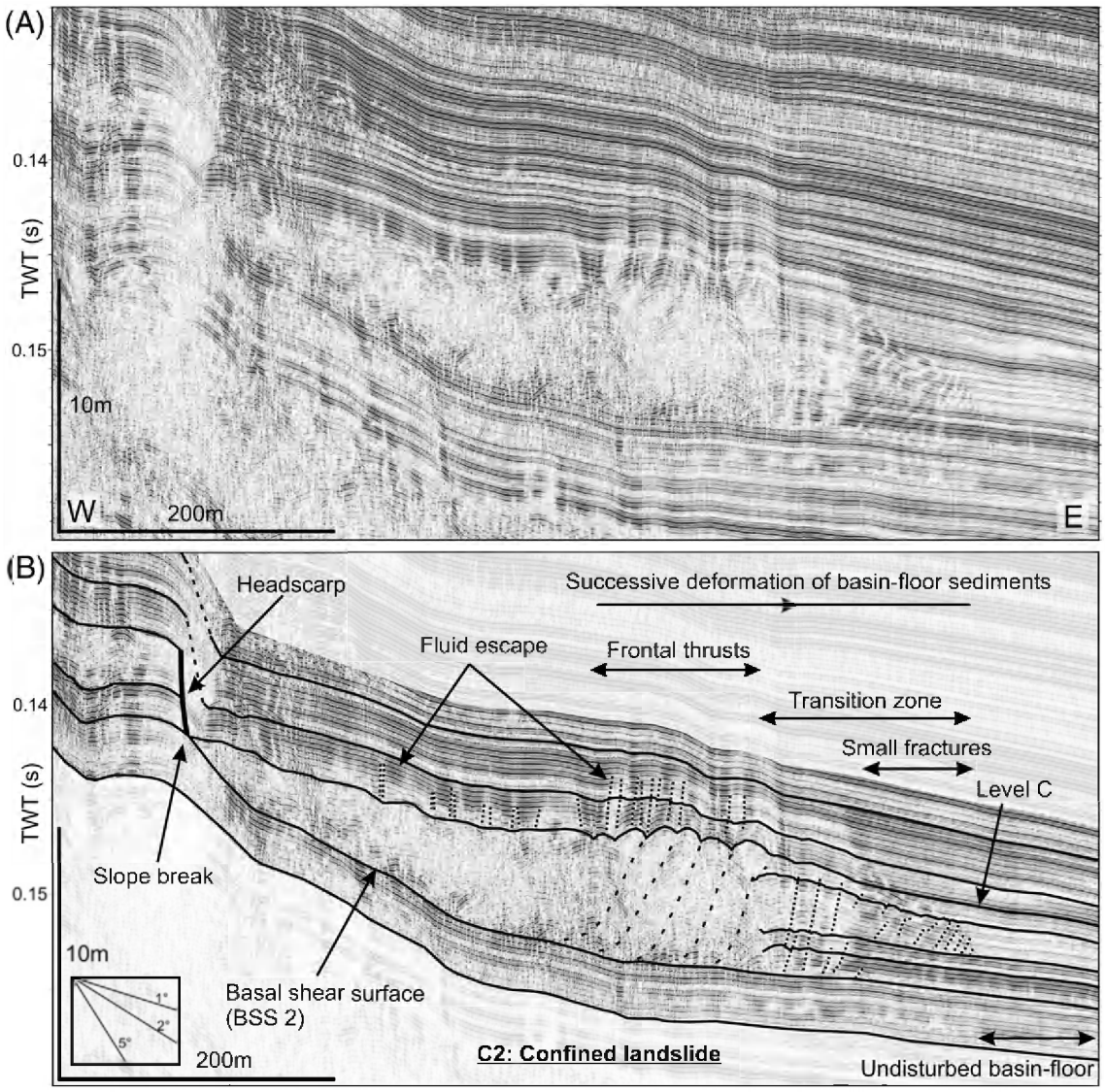

Fig. 3. Uninterpreted (A) and interpreted (B) seismic profile in Lake Challa (location on Fig. 2A) showing the detailed seismic features of a confined slide (landslide C2). The "transition zone" is located in between the frontal thrusts of the failed zone and the undisturbed basin-floor, and its thickness decreases downslope. Dashed lines: assumed frontal thrusts. Dotted lines: acoustic wipe-out zones and fractures.

bathymetry and sediment cores (e.g., Chapron et al., 1996; Chapron, 1999; Chapron et al., 2004; Ledoux et al., 2010). This case study focuses on the "Hautecombe Disturbed Unit" (HDU), which has been explained in earlier studies as a complex amalgamation of a large sublacustrine landslide (hereafter named "main lateral landslide") from the western basin slope and less voluminous landslides from the east and north of the lake basin (Chapron et al., 1996). New seismic data were obtained during a seismic equipment test survey in the winter of 2009 and allowed mapping the main lateral landslide in unprecedented detail (Fig. 5). At the western basin slopes, the headscarp of the main lateral landslide cross-cuts a ~12 m thick sedimentary sequence where the rock basement forms a discrete high and slope break. At these slopes, the lower boundary (BSS) is located at the top of the rock basement and locally within the lacustrine slope sediments. Near the basin plain periphery, the basal shear surface obliquely cross-cuts a ~10 m thick lacustrine sequence, creating a wedge-like geometry of BSS step-ups. On the basin plain, the BSS is located at multiple levels with a complex pattern of step-downs and step-ups (Fig. 5B–D). In the northern part of the main lateral landslide, the BSS progressively used shallower (younger) stratigraphic horizons as basal shear surface. In the southern part of the main lateral landslide, a BSS step-down towards an older and deeper horizon took place. The lateral continuation of the BSS levels in the undisturbed basin-plain is formed by discrete acoustic reflectors with high reflection amplitudes, which are located within the top part of Seismic Unit 5 of the seismic stratigraphy of Chapron et al. (1996). This seismic unit is probably composed of "rythmites" from the Sierroz prodelta and Rhône fan (see also Van Rensbergen et al., 1999).

Estimates of the pre-failure paleo-lake bottom (based on the thickness of adjacent unfailed sequences) allowed calculation of simple volume-balances (per unit width) on west–east seismic profiles for the main lateral landslide. Pre- and post-failure volumes are more or less in equilibrium for the area in between the headscarp and distal frontal ramp, indicating that most of the landslide mass remained in its stratigraphic confinement. Moreover, the length of the totally evacuated slope (max. 300 m) (Fig. 5C) was relatively low compared to the main lateral landslide's run-out (max. 1800 m). In its frontal part, several reflections from the undisturbed basin-plain can be tracked into the disturbed mass of the main lateral landslide (inset of Fig. 6), which indicates that these sediment packages were thrusted (and folded) but did not ramp out of their stratigraphic confinement. Recognition of such features allowed the discrimination between a

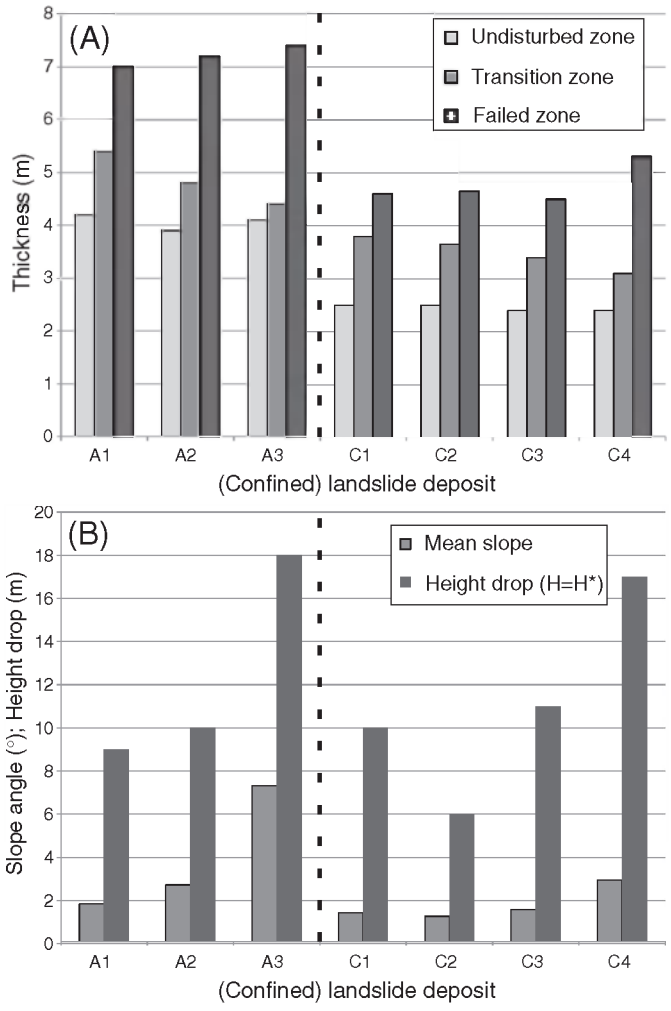

Fig. 4. A) Thickness measurements of the undisturbed zone, transition zone and failed zone of confined landslides at levels A and C in Lake Challa. B) Mean slope angle and height drop (H = H*) associated to these landslides.

compression zone, characterized by thrusts and topographic bulges, and a translation zone, characterized by few thrust faults and a rather smooth upper deposit boundary (Fig. 5C). Peculiar small-scale fractures, without vertical off-set, are present at the transition between the frontal compression zone of the main lateral landslide and the undisturbed basin-plain sediments (inset of Fig. 6). This "transition zone" can be regarded as representing the initial stage towards failure of the foreland sediments (see Section 3).

The frontal compression structures and transition zone, the small degree of landslide scar evacuation, and the volume-balances all indicate that the main lateral landslide is in effect a frontally confined landslide. It is covered by the unconfined parts of several frontally emergent landslides that originated on the northern and eastern slopes of the basin (Fig. 5B). The largest of these landslides ("axial emergent landslide" on Fig. 6) originated at the paleo-Rhône fan delta (stratigraphic interpretation: Van Rensbergen et al., 1999), where it excavated a ~20 m thick sediment sequence and ran out over the main lateral landslide deposit and the basin floor.

5. Morphometry and statistics of 96 sublacustrine landslides

5.1. Median and distribution of landslide parameters

The main dimensional and morphometric parameters of the landslides in our catalog (Table 1; Fig. 1; SI Table 5) were measured and their distributions were explored. The measured run-out distance (i.e., horizontal distance between headscarp and toe) does not represent the traveled distance of individual sediment particles or blocks which – in case of confined landslides – can be many orders of magnitude smaller than the run-out distance (e.g., Frey-Martinez et al., 2006). Several dimensional parameters are characterized by a very asymmetrical distribution (Fig. 7A/C/E) with a few data points having very large values. These strongly influence the mean parameter value, which makes the median value more suited for characterizing the "typical" landslide (Table 1). Median length, width, area and run-out distance are larger for emergent types than for confined ones, which can be explained by their free propagation and spreading of sediment mass over the lake bottom. Median volume is rather similar for emergent and confined types (306,500 m³ versus 285,000 m³) which suggests that the volume of the sediment failure is not a crucial parameter in determining the frontal development of sublacustrine landslides. Cumulative volume or run-out distributions on Log–Log plots (Fig. 7B/D) do not unambiguously fit with a logarithmic or power–law function, but rather fall in between such distribution modes. However, inverse power–law functions on reduced fractions of our dataset give a better fit (higher R^2 on Fig. 7B/D), especially when discriminating the lowest ~20% of the parameter values which are delimited by a slope-break in the cumulative distributions.

Median depth of the basal shear zone is slightly shallower for emergent landslides (1.8 m) than for confined ones (2.5 m). The distributions of the BSS depth (Fig. 7F) show that a similar range of slope sequence thicknesses can become unstable in both landslide types. Total height drop (H) for emergent landslides has a much larger median value (53 m) than that for confined types (9 m) and their distributions (Fig. 7E) show that most confined types (13 out of 17 cases) have a value of less than 10 m, while most emergent types (77 out of 79 cases) underwent a total height drop larger than 10 m. Still, for comparing the initial potential energy conditions at failure (see Section 6), the height drop H* (to the frontal ramp) should be used instead of the total height drop H (to the landslide toe).

The slope angle of frontal thrust planes in confined landslides was measured (Fig. 8A) by tracing the lateral discontinuity and vertical offset of internal reflections and by the location of topographic bulges. The thrust faults have a median angle of about 12.6° and most of their distribution falls between 8° and 18°, which is somewhat less than slope-angle values for thrust planes (10°–25°) in large-scale submarine landslide complexes revealed on 3D seismic volumes (Frey-Martinez et al., 2006). Median slope angle values for the unfailed slope (upslope of the headscarp) and for the steepest part of mass-transport are generally larger for emergent landslides (2.4°; 6.1°) than for confined landslides (1.5°; 2.5°). Emergent landslides also exhibit a wider range of maximum mass-transport slope values (0°–21°) than confined landslides (0°–9°) (Fig. 8B). It thus seems that the evacuation area for emergent landslides is generally steeper. Slope

Fig. 5. A) Seismic survey lines in the northern half of Lake Le Bourget. B) Bathymetric map (isobaths every 10 m; Chapron, 1999) with landslide features of the HDU complex and the stratigraphic positions of its basal shear surface. Gray lines indicate the position of the seismic lines in part D and Fig. 6. Arrows indicate the transport direction of the main lateral landslide (black) and several emergent landslides (gray). Compared to the L1 level, the BSS at level 2, 3 and 4 is located respectively ~1.5 m, ~2.5 m and ~8 m higher in the stratigraphy. The contemporaneous lake floor was located ~12 m higher than L1. C) Areas of total evacuation, translation or compression within the main lateral landslide. D) W–E seismic profile (C2 sparker) showing the main lateral landslide. Compression features (thrusts, topographic bulges) are mostly located above BSS step-ups. Locally, the main lateral landslide deposit (yellow) is buried by emergent landslide deposits (red).

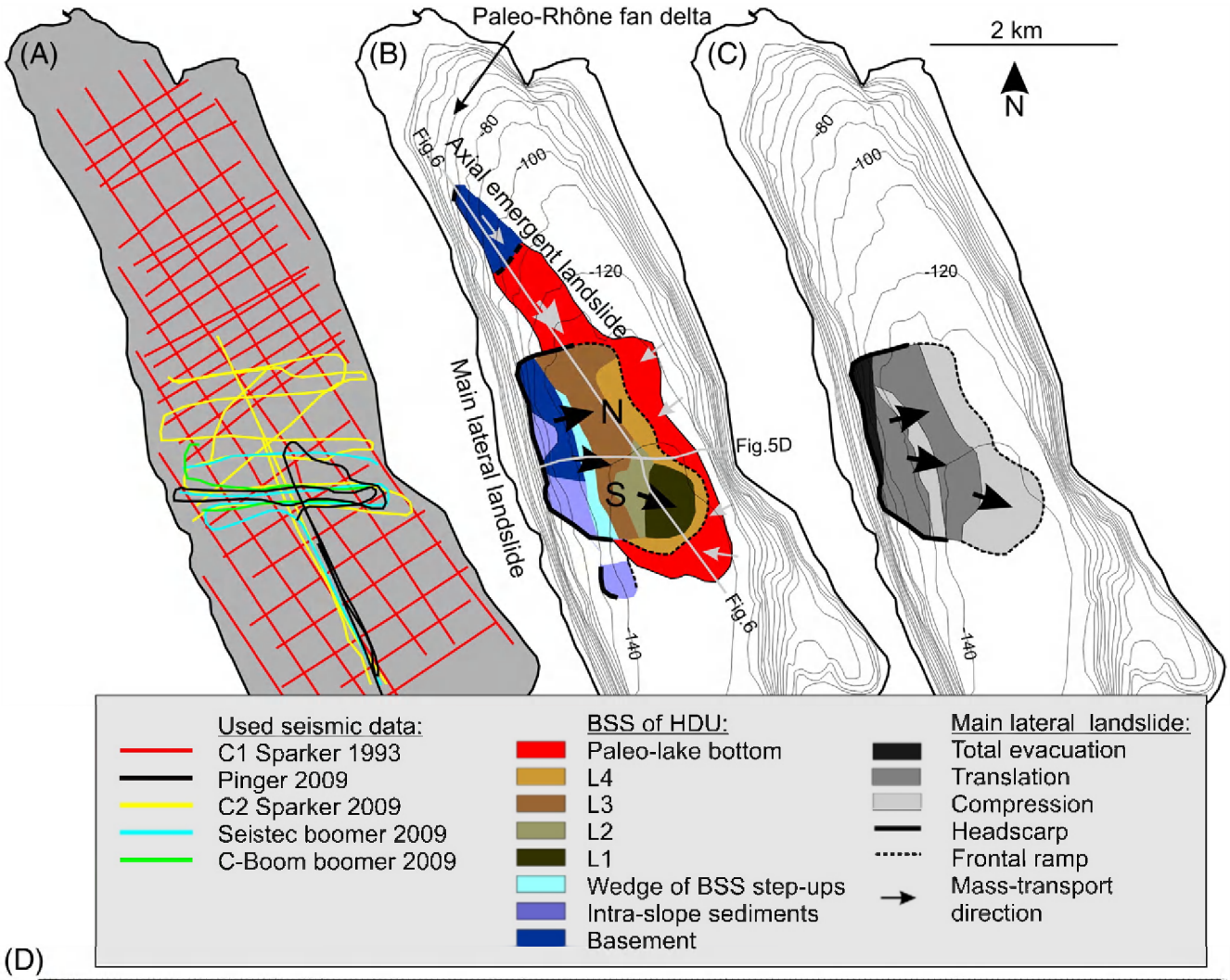
(A)
(B)
(C)
Paleo-Rhône fan delta
2 km
N
Fig.6
Axial emergent landslide
Main lateral landslide
Fig.5D
Fig.6
-80
-100
-120
-140
N
S
Used seismic data:
C1 Sparker 1993
Pinger 2009
C2 Sparker 2009
Seistec boomer 2009
C-Boom boomer 2009
BSS of HDU:
Paleo-lake bottom
L4
L3
L2
L1
Wedge of BSS step-ups
Intra-slope sediments
Basement
Main lateral landslide:
Total evacuation
Translation
Compression
Headscarp
Frontal ramp
Mass-transport direction

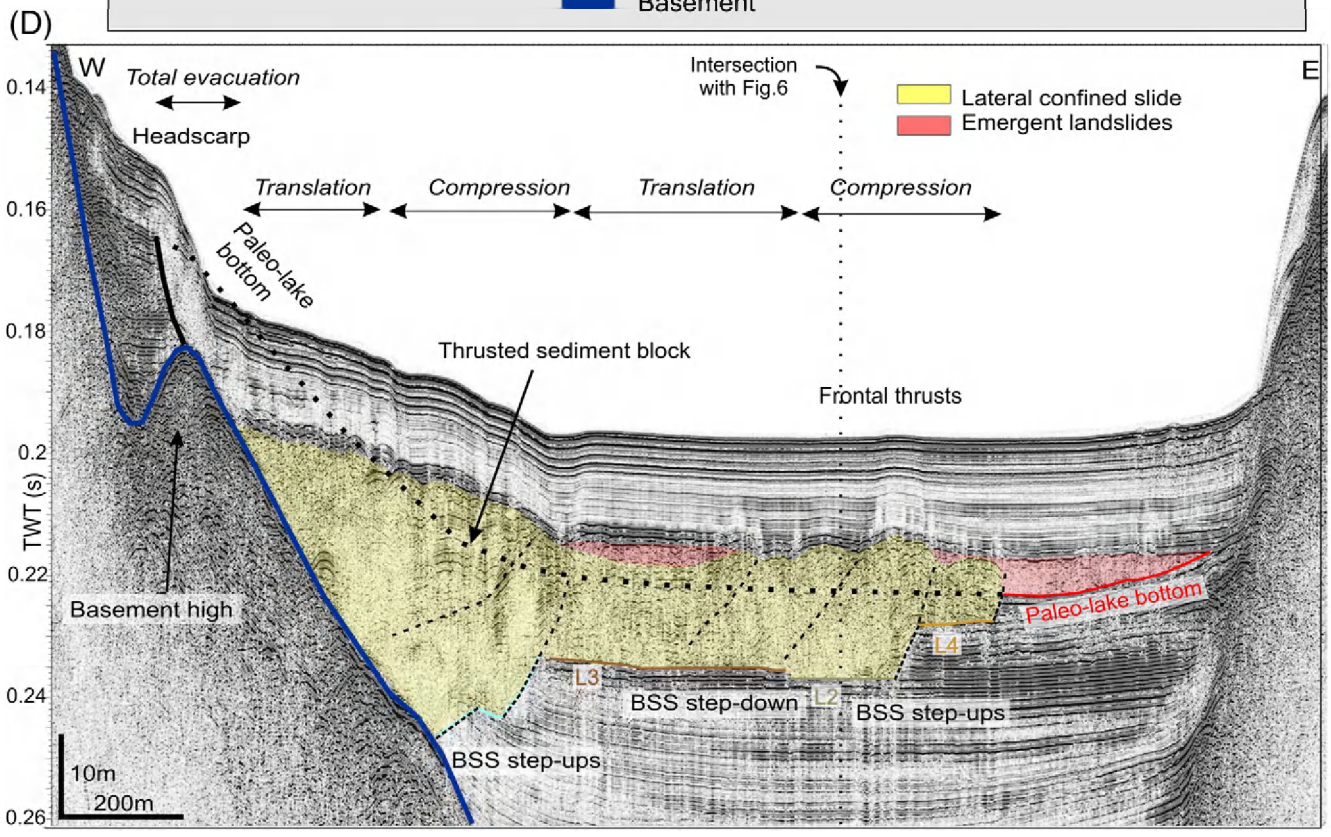
(D)
W
E
Total evacuation
Headscarp
Intersection with Fig.6
Lateral confined slide
Emergent landslides
Translation
Compression
Translation
Compression
Paleo-lake bottom
Thrusted sediment block
Frontal thrusts
Basement high
Paleo-lake bottom
L4
L3
L2
BSS step-down
BSS step-ups
BSS step-ups
10m
200m
TWT (s)
0.14
0.16
0.18
0.2
0.22
0.24
0.26

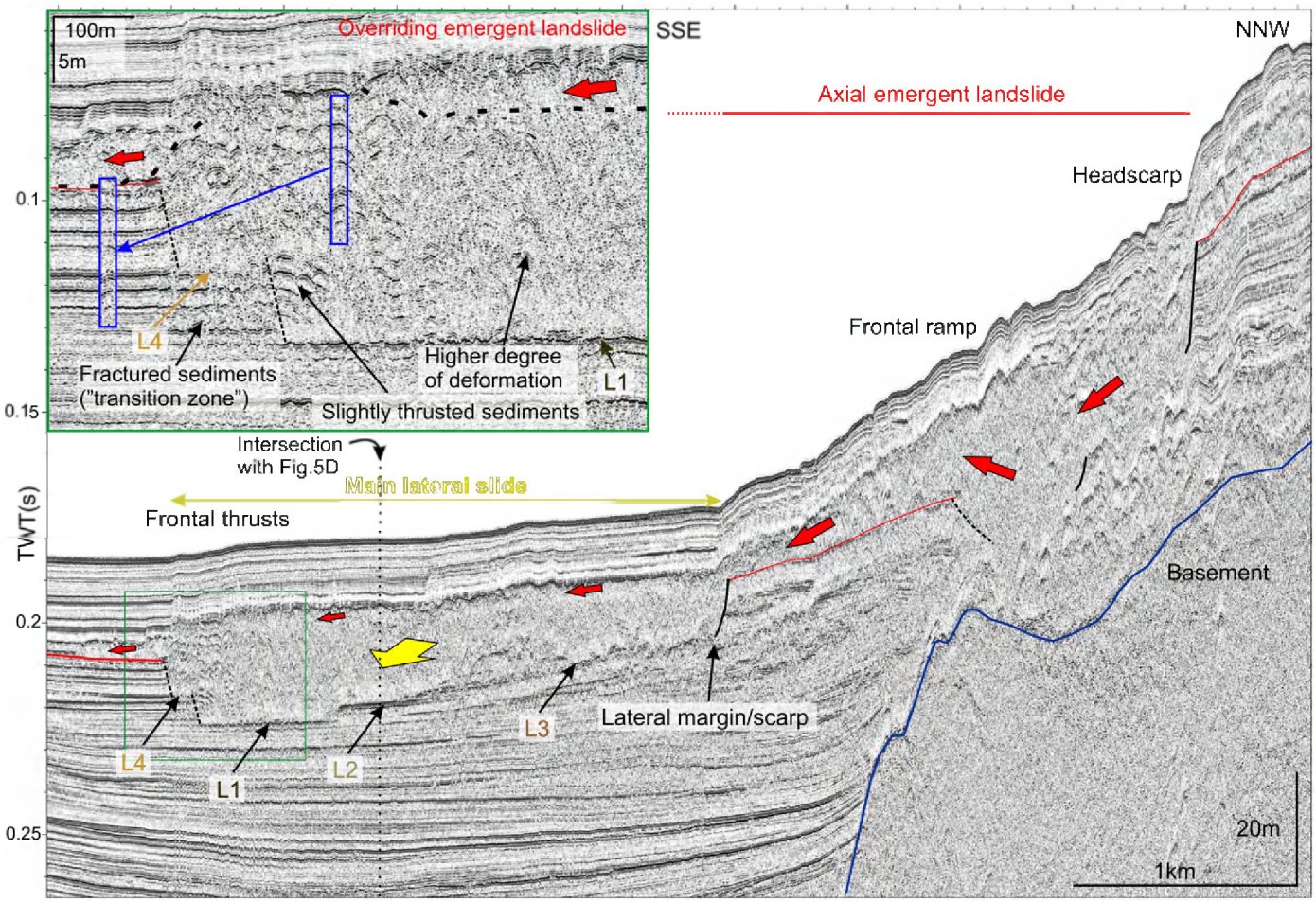

Fig. 6. NW–SE profile (C1 sparker) in Lake Le Bourget showing the main lateral landslide (yellow arrow) and axial emergent landslide (red arrows) of the HDU complex. The axial emergent landslide originated at the paleo-Rhône fan delta slope. L1–L4 represent stratigraphic levels where the BSS of the main lateral landslide developed. The red line indicates the pre-failure paleo-lake bottom (as in Fig. 5D). Inset figure (location: green box): zoom of the toe region of the main lateral landslide. A transition zone with small fractures is located in between highly-disturbed landslide sediments and the undeformed basin-plain. A correlation rectangle (copy/paste of reflection package) shows that the reflections of a coherent sediment block in the landslide body match with the basin-plain sequence.

angles at the landslide toe (Fig. 8C) are rather similar for both types (median of 0.3° for emergent landslides versus 0.4° for confined ones) and generally fall in the range of −0.2° (i.e., deposition on slightly uphill surface) and 1.6° (deposition on downhill surface).

Significant differences between the two landslide types were also found when considering some calculated ratios in between parameters. The median volume/run-out ratio is lower for emergent landslides (378) than for confined ones (851). This results from the generally higher run-out values of emergent landslides – per volume unit – due to the intrinsic ability of (freely flowing) emergent landslides to develop a larger translation of individual sedimentary elements. The median value for the total height drop/depth basal shear surface is much larger for emergent landslides (30.2) than for confined ones (4.0), which is due to the generally larger total height drop for emergent landslides. This ratio possibly characterizes the potential gravitational energy of a landslide compared to the potential energy needed to emerge at the frontal ramp and might be of key importance in the frontal development of landslides (see Section 6). The total height drop/run-out ratio (Fig. 8D) is typically used to characterize the mobility of a mass movement (Hampton et al., 1996; Locat and Lee, 2002). In general, the most mobile landslides are characterized by low values of this ratio. However, in our study, the median value for this ratio is higher for the emergent types (0.048) than for the confined ones (0.017) due to the generally much larger total height drop involved with emergent landslides. These median values would suggest that emergent types would have a lower mobility than confined landslides. Contrarily, landslides with a confined frontal emplacement intrinsically have a very low mobility and, therefore, their mobility must be assessed by measuring the height drop and run-out undergone by the center of gravity (Legros, 2002) instead of the total height drop/run-out ratio of the landslide complex.

These median values and distributions in our sublacustrine landslide catalog provide a first insight in to the differences between confined and emergent landslides.

5.2. Relationships between landslide parameters

Correlation coefficients were calculated in between all measured morphometric parameters and ratios in order to reveal some possible relationships between them. In this study, the commonly used Pearson correlation coefficient was not used, as this requires that the parameters be normally distributed (Davis, 1986). Instead, we opted to calculate the non-parametric Spearman's rank correlation coefficient (Spearman's rho) that does not require any specific frequency distribution of the variables. The Spearman's rank correlation coefficient indicates if parameters vary together, but these should not necessarily relate in a linear way. Some strong (>0.5) to

Table 1
Median values for morphometric parameters and ratios of frontally confined and emergent sublacustrine landslides. "N" is the number of landslides included in the analysis.

	Confined		Emergent	
	Median	N	Median	N
Water depth of headscarp (m)	108	17	89	78
Water depth of landslide toe (m)	118	17	128	79
Total height drop H (m)	9	17	53	78
Water depth of frontal ramp (m)	118	17	116.5	61
Length of landslide deposit (m)	280	17	410	79
Width of landslide deposit (m)	250	13	490	58
Thickness of unconfined part (m)	X	X	1.2	79
Length/width	1.17	13	1.27	58
Total height drop/run-out	0.017	17	0.048	68
Length/thickness unconfined	X	X	370	79
Area (m²)	70 000	13	223 000	58
Volume (m³)	285 000	12	306 500	54
Depth basal shear surface (m)	2.5	17	1.8	36
Slope angle of frontal thrusts (°)	12.6	9	X	X
Slope angle at toe (°)	0.40	15	0.30	77
Slope angle upslope headscarp (°)	1.5	16	2.4	36
Max. slope angle of mass transport (°)	2.5	16	6.1	75
Slope angle of snout (°)	X	X	1.8	71
Run-out (m)	390	17	800	69
Headscarp height (m)	2.5	16	4.15	32
Volume/run-out (m²)	851	12	378	51
Total height drop/depth BSS	4.00	17	30.16	36

X: not applicable.

very strong correlations (>0.9) were found (SI Tables 3 and 4), of which the underlying reason can be explained straightforwardly. For example, the large correlations between volume on the one hand, and length, width, area and unconfined thickness on the other hand are evident because all these parameters are inherent parts of the general formula for the volume calculation of a body. Correlations that could not be explained in this way were examined using scatter plots. The R^2 value was used to characterize the goodness of fit of a regression line to the empirical data values. Despite the rather small quantity of cataloged confined landslides (n = 17), we still consider this a valuable dataset for making comparisons with the emergent landslides as i) it covers more or less the same dimensional range (Volume: ~10^4–10^8 m³), and ii) adding datapoints would not produce totally different relationship values, correlation coefficients or R^2 values. Obviously, more datapoints would strengthen the reliability (statistical power) of the obtained relationships, especially for confined landslides with volumes of 10^6–10^7 m³ as these are not present in our catalog.

A relationship was found between deposit area and volume for both emergent and confined landslides (Fig. 9A). Both datasets show a very good fit (R^2 emergent: 0.939; confined: 0.942) to power functions $V_L = 0.0744A_L^{1.241}$ (emergent) and $V_L = 0.0727A_L^{1.330}$ (confined). Volume also relates to run-out distance (Fig. 9B) with a good fit (R^2 emergent: 0.734; confined: 0.864) to power functions for both emergent and confined landslides. Rather moderate to poor fits ($0.2 < R^2 < 0.6$) to power functions exist between run-out distance on the one hand and total height drop (Fig. 9C), unconfined thickness (Fig. 9D) and headscarp height (Fig. 9E) on the other hand. This suggests that landslide run-out essentially depends on the failing slope volume and not as much on the total height drop. This also explains the very low correlation (low R^2 values) between run-out ratio (H/Run-out) and volume (Fig. 10A), as the total height drop parameter simply introduces scatter to the data (see Legros, 2002 for discussion). Confined landslides principally plot in the lower part of the data cloud were a high mobility is assumed, which contradicts their confined emplacement (Section 5.1).

Plots which include the height drop (H*; to the frontal ramp) parameter (Figs. 9C and 10B) expose the most striking differences between frontally emergent and frontally confined landslides. The plot of height drop H* compared to the depth of the BSS (Fig. 10B) reveals distinctive chart areas were frontally emergent or confined landslides are present. For landslides with a BSS shallower than 5 m, frontal emergence took place for height drops larger than approximately 15 m. For a BSS depth of 10 m, frontally emergent landslides had a height drop of more than 35 m.

Most headscarps are located at a downslope-steepening slope break in the stratigraphic level acting as BSS. These slope breaks range between 0° and 7° (Fig. 9F), with most values in between 1° and 2° (median: 1.7°). This means that rather subtle changes in slope gradient can actually delimit the evacuation zone from the zone in which the sedimentary sequence did not fail and remained in position. Furthermore, the unfailed slope values indicate that – in our catalog – slopes with a gradient up to 3°–4.5° can remain stable even though their downslope basal support was suddenly removed by slope failure.

Although gravity is the driving force for landslide development and landslides are forced to travel downslope on the existing topography, absolute slope values correlate poorly with most other parameters (SI Tables 3 and 4) and therefore do not noticeably influence the occurrence and dimensions of sublacustrine landslides. A similar independency from slope angle was also found in submarine landslide catalogs (McAdoo et al., 2000; Hühnerbach et al., 2004) and suggests that other factors mainly govern the initiation and propagation of subaqueous landslides.

6. Factors controlling the frontal emplacement style of sublacustrine landslides

An important challenge is to reveal which mechanisms control why certain landslides propagate in a frontally confined manner while others are able to ramp out on to the contemporaneous lake/sea floor. Based on local case studies, several explanations have been put forward during the past decades. Trincardi and Argnani (1990) suggested that the frontal confinement of the Gela landslide was controlled by the presence of a morphostructural obstacle, which prevented further translation. Huvenne et al. (2002) identified a large, buried submarine confined landslide on a 3D seismic dataset, and hypothesized that its emplacement style was caused by a combination of abrupt pore-pressure dissipation from the BSS and a rather low regional slope angle. Frey-Martinez et al. (2006) proposed that thicker landslides simply require more energy to emerge at the frontal ramp, and thus tend to remain locked in their frontal confinement.

In the present study, descriptive statistics on morphometric parameters of sublacustrine landslides confirmed the discriminative patterns between frontally confined and emergent landslides that were found in the case study on Lake Challa (Case study 1). Height drop H* (in between headscarp and frontal ramp), depth of basal shear surface and slope angle of mass transport all seem to exert some control on the frontal emplacement style. The clearest discrimination between the two end-members was provided by the scatter plot of depth BSS against H* (Fig. 10B). The observed distribution can be explained by the following mechanical model, which is partially based on the hypotheses made by Frey-Martinez et al. (2006).

Failing slope masses can become emergent if their gravitational potential energy is high enough to overcome the potential energy requirements to ramp out of their stratigraphic position. Thicker landslides are more likely to remain locked in the confined stage due to their lower center of gravity (CoG) compared to the lake bottom and due to higher energy demands for full frontal ramping. Furthermore, H* essentially determines the gravitational potential energy of the initial landslide mass and thus we can consider H* as the main driving parameter for the development of frontal emergence and depth BSS as the main restricting parameter. Thus, for any given H*, the proportion between the parameters H* and depth BSS will mainly determine whether a landslide becomes emergent or not

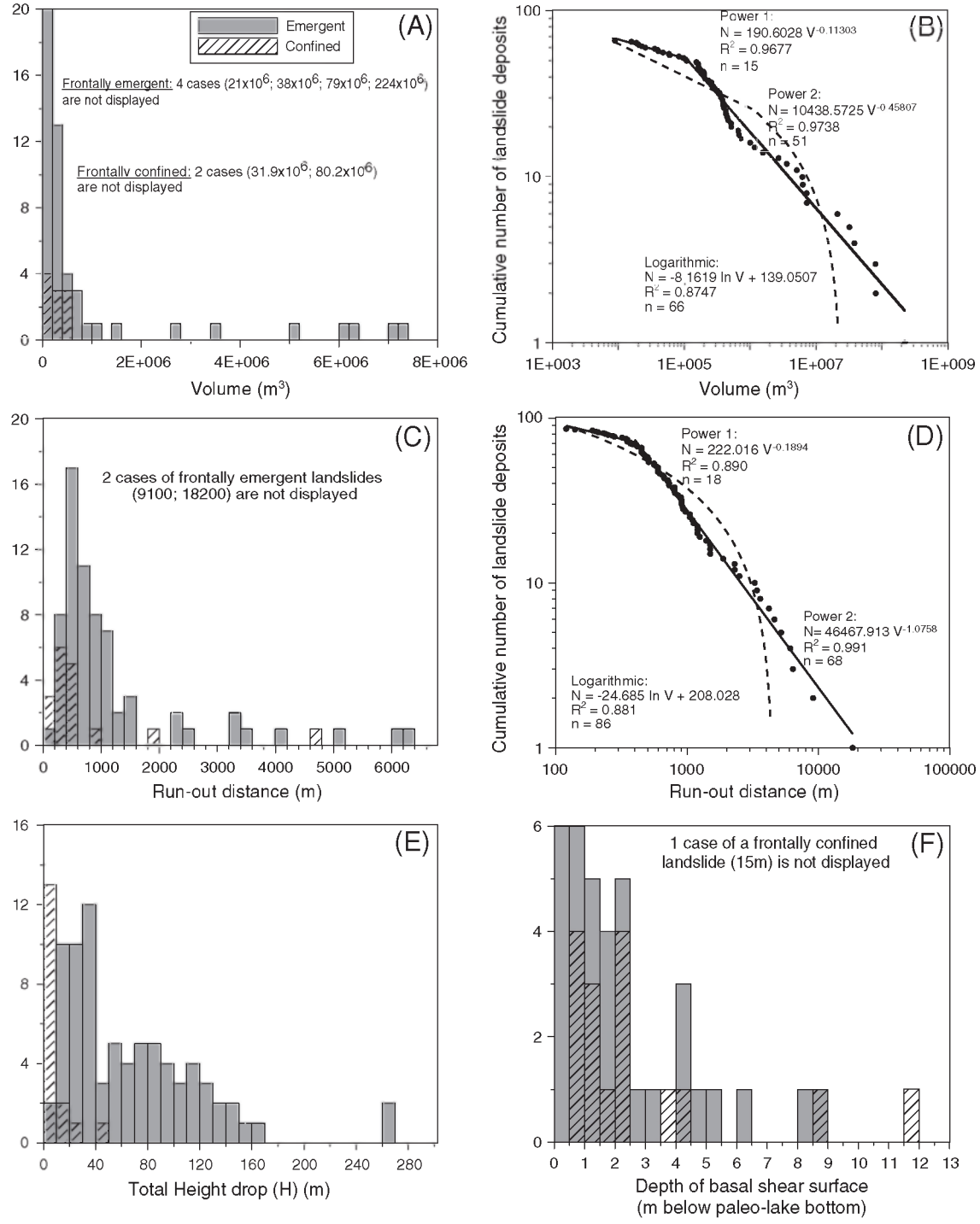

Fig. 7. A, C, E, and F) Histograms of morphometric parameters for sublacustrine landslides. The vertical axis in the graphs shows the number of landslides. Confined slides are indicated by hatched columns. For illustrative clarity, some very large values were not illustrated, but were still included in the parameter calculations. B and D) Cumulative distribution of sublacustrine landslide volume and run-out. n: number of landslides.

(Fig. 10B). In effect, both parameters principally determine the height of the CoG of the failed mass above (or below) the top of the frontal ramp (Fig. 11B). The larger this height difference, the greater the landslide's ability to ramp out its frontal confinement (Fig. 11A). According to this model, frontal emergence is not possible if the CoG is below the frontal ramp top. Once a landslide is able to ramp out, most of the slide scar gets evacuated as the unconfined propagation allows the upper parts of the failing slope to accelerate and gain kinetic energy, creating an uninterrupted process of frontal emergence.

During confined landsliding on a downslope-decreasing slope gradient, mass potential energy gets lost because of the progressive lowering of the CoG of the landslide mass compared to the top of the frontal ramp. Consequently, less potential energy is available to ramp out, and – in spatially uniform deposits – the landslide will exclusively propagate further in a confined manner, progressively executing less lateral stress on the foreland. As shear strength generally increases with burial depth (e.g., Bartetzko and Kopf, 2007), we speculate that this stress attenuation can lead to distal step-ups of the BSS. This

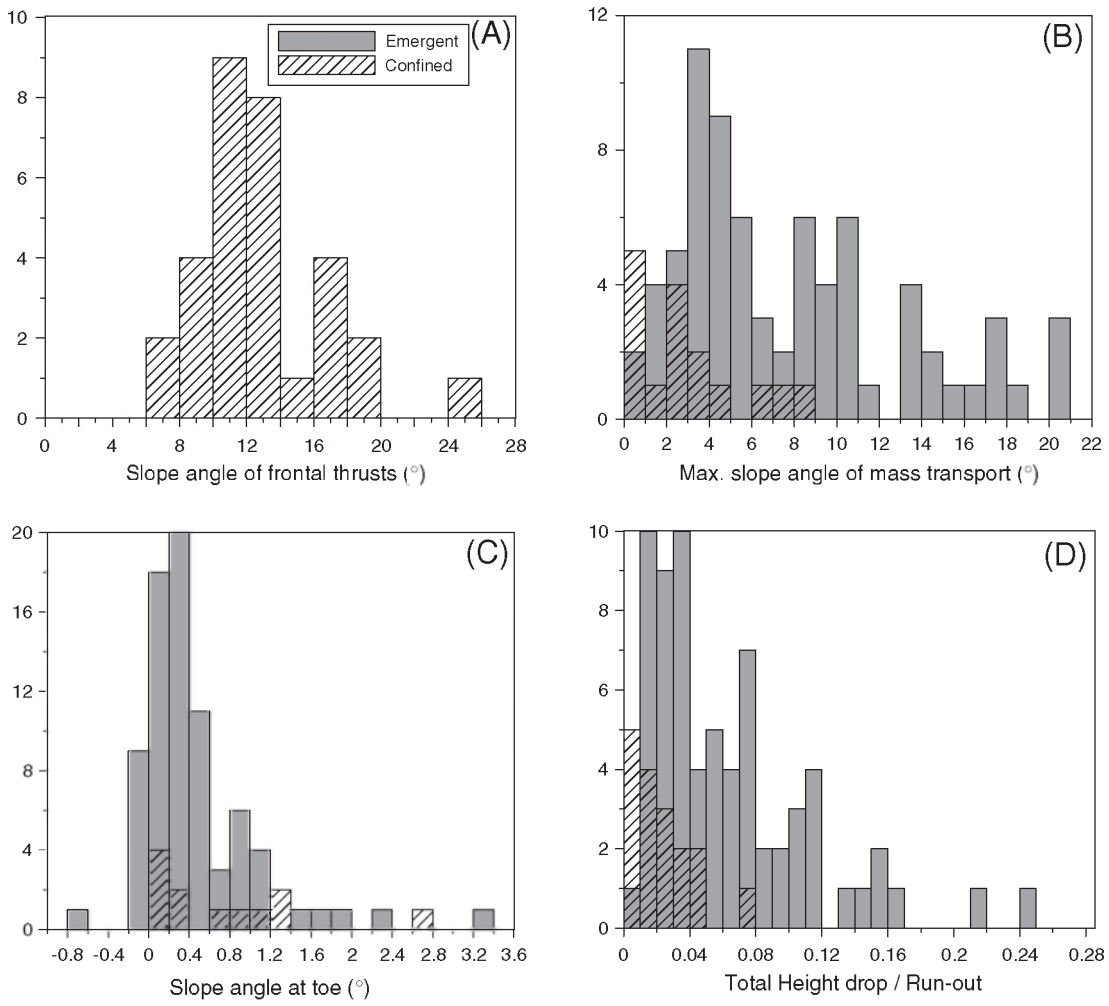

Fig. 8. Histograms of morphometric parameters (and ratios) for sublacustrine landslides. The vertical axis in the graphs shows the number of landslides. Confined slides are indicated by hatched columns. For illustrative clarity, some very large values were not illustrated, but were still included in the parameter calculations.

might explain the discrete BSS step-ups observed in the northern part of the main lateral landslide in Lake Le Bourget (Case study 2; Fig. 5B) and the shallow "transition zone" at the front of confined slides in Lake Challa (Case study 1; Fig. 3). Consequently, the orientation of such BSS step-ups should be mostly located perpendicular to the main landslide direction (Fig. 5B). Development of BSS ramp-and-flat geometries in submarine landslide complexes has been attributed to variability in the geotechnical properties of the stratigraphic sequence (Frey-Martinez et al., 2005; Solheim et al., 2005; Bull et al., 2009). Geotechnical studies showed that BSS's can either develop at the boundary between major sedimentary units with different shear strength and/or pore pressure regimes (e.g., Storegga Slide: Leynaud et al., 2007; landslides in Lake Lucerne: Strasser et al., 2007), or at intercalated layers of relatively coarse sediments which are prone to earthquake-induced liquefaction (e.g., coarse silt to sand: Dan et al., 2009; sandy tephra: Harders et al., 2010). Consequently, the thickness of the failed section is mainly controlled by these (stratigraphic) preconditioning factors, more than by the magnitude of the ultimate triggering mechanism (e.g., strong earthquake). In the main lateral landslide in Lake Le Bourget, this lithological influence is reflected by the coincidence of "flat" BSS parts with discrete reflectors with high reflection amplitude. Strachan (2002) postulated that local down-cutting of the BSS may indicate a change from easy slip along the BSS towards reduced slip. In the distal southern part of the main lateral landslide in Lake Le Bourget, eastward driving stress would have been relatively low due to the large distance from the failed slope. Possibly, the small-scale step-downs there might result from the additional buttressing effect executed by the slightly west-ward dipping basin-floor sediments as the deformation front was approaching the eastern lake basin flank (Fig. 5B).

The case study on Lake Challa (Case study 1) illustrates that downslope lateral stresses in the toe region of confined landslides can be accommodated in a complementary way by either partial frontal ramping and/or compression (slope-parallel compaction) of the foreland (Fig. 4). For the spatially uniform deposits of Lake Challa, it can be assumed that – within the same stratigraphic section – the intrinsic strength of the nearly-flat foreland is similar for different landslides. Therefore, the style of confined emplacement must be primarily controlled by the downslope driving force. For larger values of height drop H*, propagation of the failed mass becomes more emphasized on frontal ramping than on foreland compression (Fig. 11A). As height drop increases above a critical value, the failed mass effectively ramps out creating an emergent-type landslide. As the foreland is no longer stressed then, we do not expect to have a prominent "transition zone" associated to emergent landslides. Thus, a continuous spectrum of landslide types – characterized by their relative degree of either frontal ramping or foreland compression – can be ascribed to the two end-member model of Frey-Martinez et al. (2006).

Our landslide catalog shows that the occurrence of confined landslides seems to be restricted to slopes angles lower than 8°–9° (Fig. 8B). Steeper slopes (with considerable length) exclusively

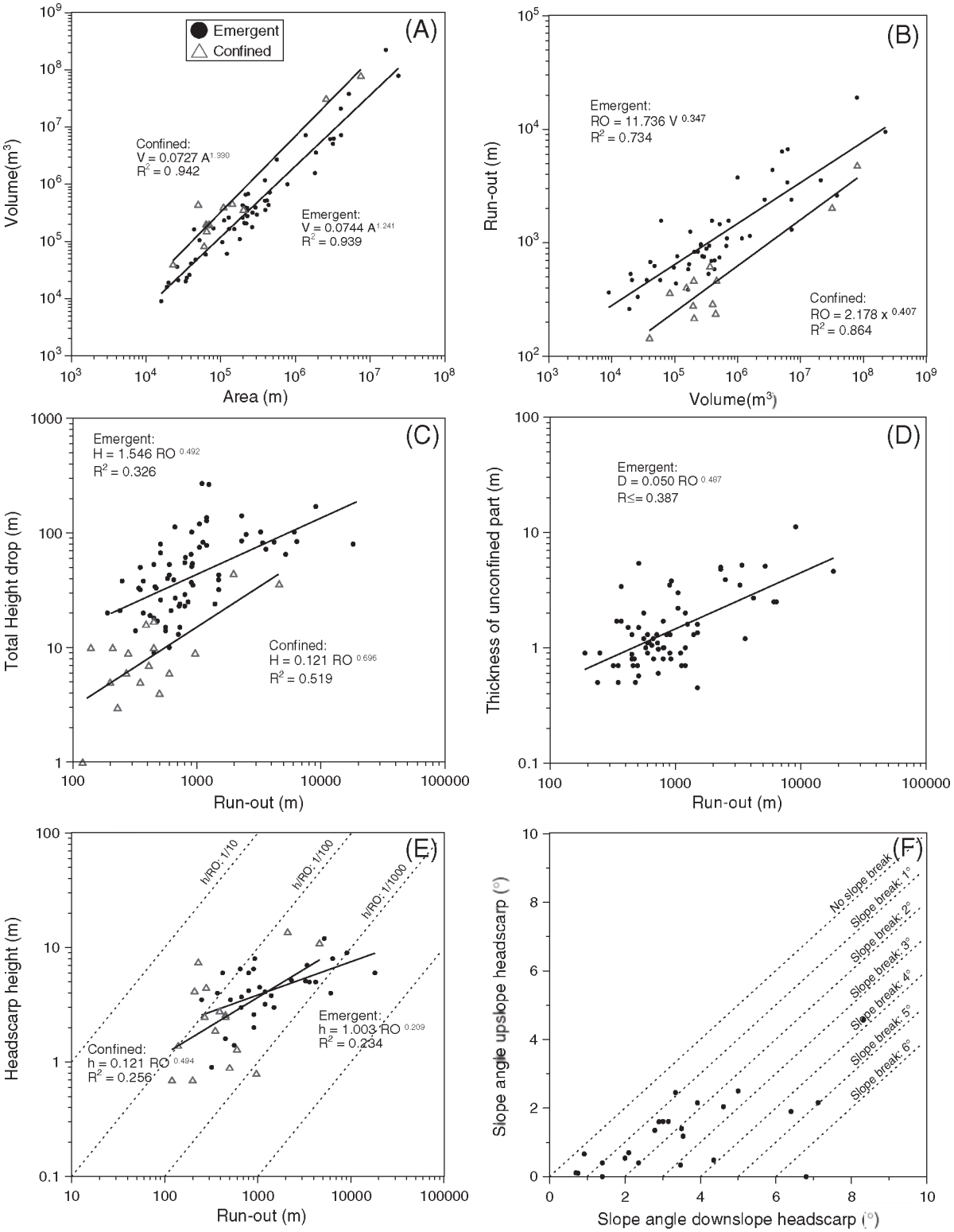

Fig. 9. Scatter plots of morphometric parameters for sublacustrine landslides. Confined slides are indicated by triangles.

generated frontally emergent landslides, possibly due to a reduced static and kinetic friction along the BSS and hence more efficient potential energy transfer. Gradient changes of the slope profile also seem to be of critical importance as headscarps form at downslope-steepening slope breaks (Fig. 9F). Frontal ramps are generally located in the basin-plain, close to the lower slope break (decreasing slope gradient), which induces a buttressing effect (Mandl and Crans, 1981). Thus, changes in slope gradient strongly control the length of the slope section that was involved in slope failure and its height drop H*.

In summary, two principal parameters determine the frontal emplacement style of landslides: i) the shape of the slope profile which controls the location of headscarp and frontal ramp (and thus H*), and ii) the geotechnical properties of the sedimentary sequence

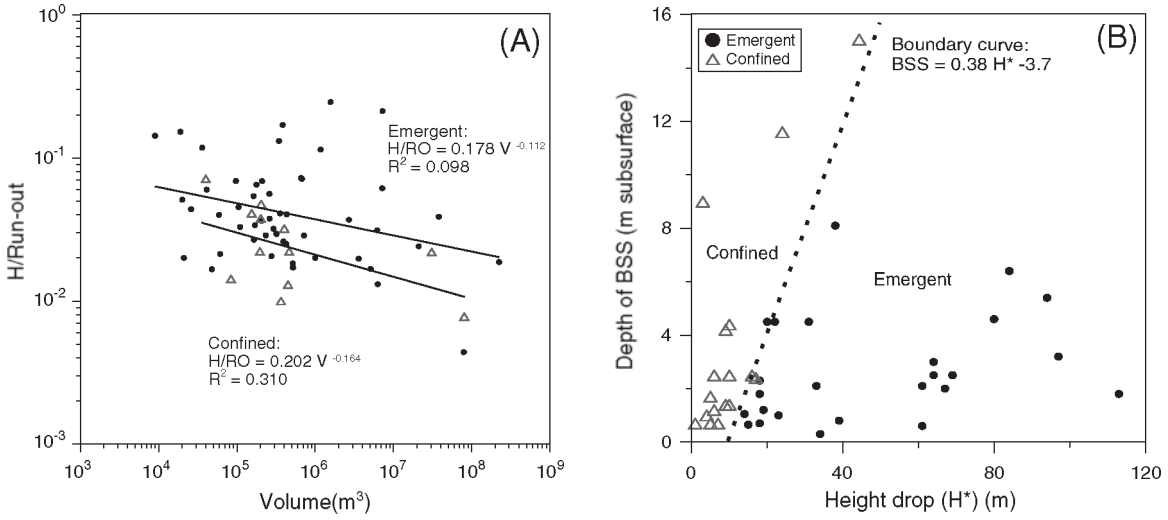

Fig. 10. Scatter plots of morphometric parameters for sublacustrine landslides. Confined slides are indicated by triangles.

which control the depth of the BSS. This underlines the potential to effectively predict the frontal emplacement style of future subaqueous landslides, which is of high importance for natural-hazard assessments, as the consequences of frontally confined and emergent landslides likely differ significantly. For example, the unconfined part of frontally emergent landslides is able to develop into high-speed turbulent sediment flows that can travel large distances and might cause large infrastructural impacts (e.g., Grand banks disaster; Piper et al., 1988), while confined landslides do not transform into other kinds of gravitational mass movements. Also, confined landslides have a much smaller displacement of mass (and thus water) and probably a much lower initial acceleration and maximum velocity, and therefore their tsunamogenic potential (Harbitz et al., 2006) is expected to be significantly lower than for emergent landslides. A better knowledge about the kinematic factors of confined landslides is however needed to effectively quantify their (reduced) tsunami hazard.

7. Dimensions, disintegration and mobility: comparison with submarine landslides

Comparison of our sublacustrine landslide dataset with statistical studies on submarine landslides is crucial for determining the value and significance of the inferred relationships. Our lacustrine catalog principally emphasizes on the landslide deposits, while McAdoo et al. (2000) and Hühnerbach et al. (2004) cataloged the dimensions of the entire submarine mass-transport complexes (i.e., the sum of the

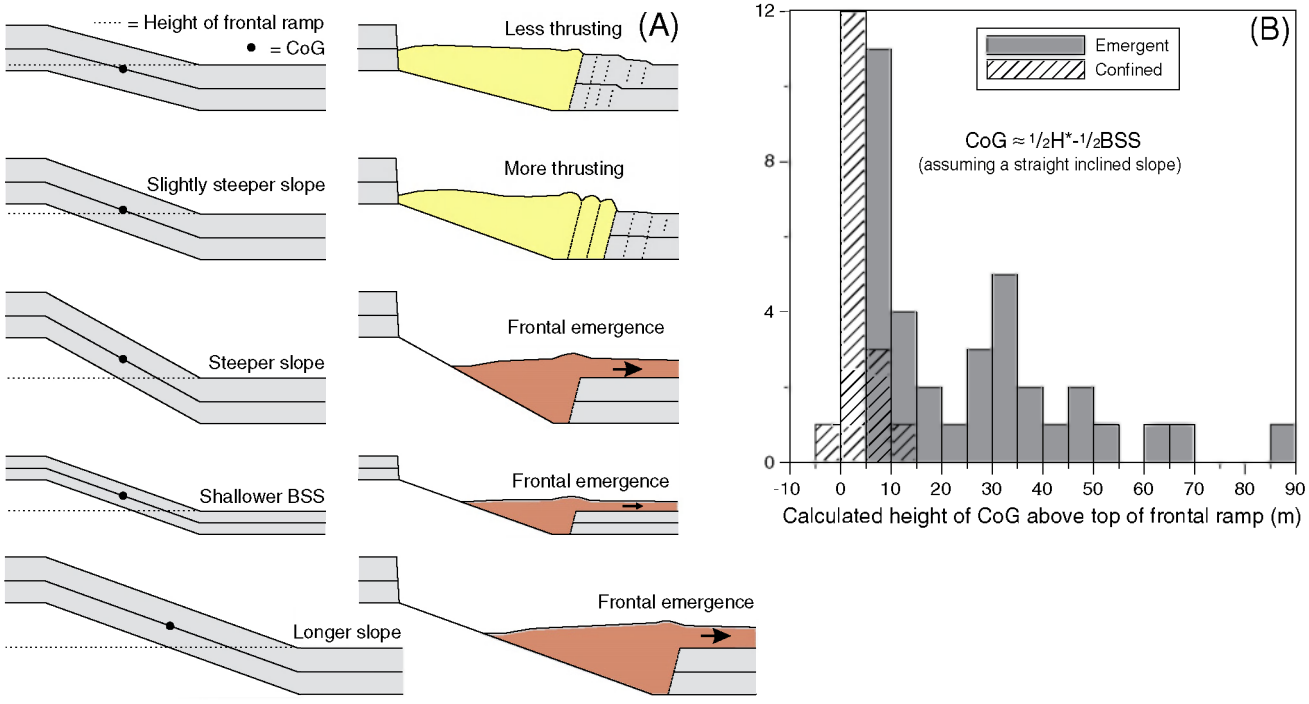

Fig. 11. A) Schematic illustration of the factors (slope angle, depth BSS, and slope length) controlling the height of the CoG above the frontal ramp and thus the frontal emplacement style of subaqueous landslides (yellow: confined; red: emergent). These controlling factors are interchangeable, so that steeper slopes, shallower excavation or longer slopes all produce more emphasis on frontal thrusting and emergence. B) Simplified calculation of CoG height above the frontal ramp for cataloged sublacustrine landslides. The vertical axis in the graphs shows the number of landslides.

landslide evacuation area and depositional area). Moreover, Chaytor et al. (2009) studied the size distribution of the submarine excavation areas without taking into account the depositional area. Therefore, it is important to keep these methodological differences in mind when comparing the different landslide catalogs.

Diverse size distribution models have been proposed for explaining the occurrence of submarine landslide features at ocean margins: i) inverse power–law distributions (Issler et al., 2005; ten Brink et al., 2006; Micallef et al., 2007), ii) log-normal distributions (Chaytor et al., 2009; ten Brink et al., 2009), and iii) logarithmic distributions (Issler et al., 2005). Distribution of volume and run-out of sublacustrine landslides showed best fits to inverse power laws (Fig. 7B and D) on truncated portions of the data, a phenomenon that is usually explained by undersampling of specific magnitude ranges (ten Brink et al., 2006). In this view, the relative absence of small landslides might result from under-recording as these could be located in between the 2D seismic survey lines (depending on the survey grid spacing; typically 50–500 m) or fall below vertical seismic resolution (depending on the seismic system). Conversely, the relative absence of small landslides might also be a real physical phenomenon characteristic for the subaqueous slope failure process. In effect, a certain critical mass (static load) above a potential failure plane is required to overcome the resisting forces for failure (e.g., Strasser et al., 2007) and therefore the development of very small landslides (shallow failures) may be unlikely.

The regression line exponent for sublacustrine landslide volume (0.458; power fit 2 on Fig. 7B) is quite similar to the exponent of the power–law function applied on debris lobe deposits within the Storegga Slide complex (0.44), as documented by ten Brink et al. (2006) based on data in Haflidason et al. (2005). This exponent value (<1) signifies that the few large landslides are relatively more important for transporting sediment to the deep basin than the large amount of small landslides. It is considerably lower than for most other landslide catalogs, where exponents up to 1.3 were documented (e.g., Chaytor et al., 2009). For submarine carbonate rock failures and subaerial rockfalls, the inferred low exponent was attributed to their high cohesion and/or friction coefficient (Dussauge et al., 2003; ten Brink et al., 2006). However, for subaqueous landslides in unconsolidated sediments, compositional variability cannot be invoked for explaining the exponent values at different segments along the US Atlantic Slope (Chaytor et al., 2009), or the low values of the Storegga debris lobes and sublacustrine landslides. Ten Brink et al. (2009) proposed that maximum landslide size along the US Atlantic margin might be related to earthquake magnitude, the distribution of which can be approximated by the Gutenberg–Richter frequency–magnitude relationship. This would mean that landslide size distributions along the US Atlantic margin primarily reflect the slope failure triggering mechanism. In Chilean lakes, however, it is inferred that some megathrust earthquakes produced extensive landslides, while other similar shaking events did not (Moernaut et al., 2007; Moernaut et al., 2009). There, slope sediments on failed slope segments probably did not accumulate fast enough to reach the critical thickness for failure during the subsequent megathrust earthquake. For Lake Challa, it has been suggested that landslide events were mainly generated when lake-level drops lowered the overall slope stability by creating excess pore water pressure (Moernaut et al., 2010). Consequently, for most of the cataloged sublacustrine landslides, failure size does not relate directly to earthquake strength, but is strongly controlled by conditions of pore water pressure, the availability of "weak layers" and the static load executed on them. Possibly, this static load control promotes the development of large failures over small ones and is reflected in the low exponent values of landslide size distributions in lakes.

Insights in scaling behavior of subaqueous landslides can be important in terms of submarine hazard management, as incomplete landslide catalogs can be extrapolated to estimate the frequency of large-scale hazardous landslide events. Power–law distributions may imply spatial scale invariance, which could be explained by self-organized criticality in a geomorphic system (e.g., the Storegga Slide: Micallef et al., 2008). However, power–law scaling of landslide sets may also reflect the morphological characteristics of the affected area (ten Brink et al., 2009). Accordingly, power–law distributions in our lacustrine landslide dataset are best explained by the typical confined morphology of lake basins and its influence on landslide size. It thus seems that size-distributions in lake basins are not suited for investigating the processes and initiation mechanisms of subaqueous slope failure, and for making predictions about failure size probabilities. Such information can be gained by investigating extensive areas of uniformly-dipping slopes that can be found in the submarine realm (e.g., ten Brink et al., 2009).

The area/volume relationships for the sublacustrine landslide deposits in the present study (emergent exp.: 1.241; confined exp.: 1.330) show that the more extensive deposits are generally thicker. These values are considerably higher than the exponent (exp.: 1.032) derived from debris lobes within the Storegga Slide complex (ten Brink et al., 2006). This contrast might be explained by the typical morphological confinement – and thus reduced landslide depositional area – of the lacustrine basins, promoting the accumulation of relatively thicker landslide deposits. It is not useful to compare with the reported exponent values derived from submarine carbonate rock failures of Puerto Rico (exp.: 1.292) (ten Brink et al., 2006) and U.S. Atlantic margin failure zones (exp.: 1.099) (Chaytor et al., 2009) as these studies documented the landslide scar area instead of the landslide deposits, and therefore providing information about failure parameters (depth of slide plane, etc.) rather than of depositional processes.

Several morphometric parameters (and ratios in between them) suggest that frontally emergent landslides in lakes (and fjords) tend to be characterized – in general – by a higher mobility and larger disintegration than ocean margin landslides:

i) Lower ratios of headscarp height to run-out distance. McAdoo et al. (2000) show values up to ~0.1 for submarine landslides, while those of emergent sublacustrine landslides have are maximum 0.0143 (Fig. 9E). Most values for "disintegrative" landslides in the catalog of McAdoo et al. (2000) and the emergent sublacustrine landslides fall in the same range (0.01–0.001).
ii) Higher run-out distance per volume (per unit width) (Fig. 12). Emergent sublacustrine landslides plot above the extrapolated regression lines found for debris lobes in the Storegga Slide or the data cloud of submarine landslides in the COSTA-database (Issler et al., 2005).
iii) Lower run-out ratio per volume (Fig. 13). Emergent sublacustrine landslides plot below the upper bound for submarine landslides from Hampton et al. (1996) and several of them plot below the lower bound for subaerial quick clay landslides (Edgers and Karlsrud, 1982). The power fit curve plots very close to the lower bound for submarine landslides proposed by Edgers and Karlsrud (1982). Although the significance of the run-out ratio regarding landslide mobility is questionable (Legros, 2002), this plot might still aid in comparing different landslide datasets.
iv) Larger reduction of deposit thickness compared to the failed slope section (Fig. 14). Landslides on the Eastern Atlantic Margin (Hühnerbach et al., 2004) have small values (or even absence) of deposit thickness reduction and plot well above the power function of emergent sublacustrine landslides and the data cloud of fjord landslides.

Variation in sediment composition (i.e., sand-to-clay ratio) of the failed mass has been put forward in explaining flow behavior and mobility of submarine debris flows (Elverhøi et al., 2010). Clay-rich

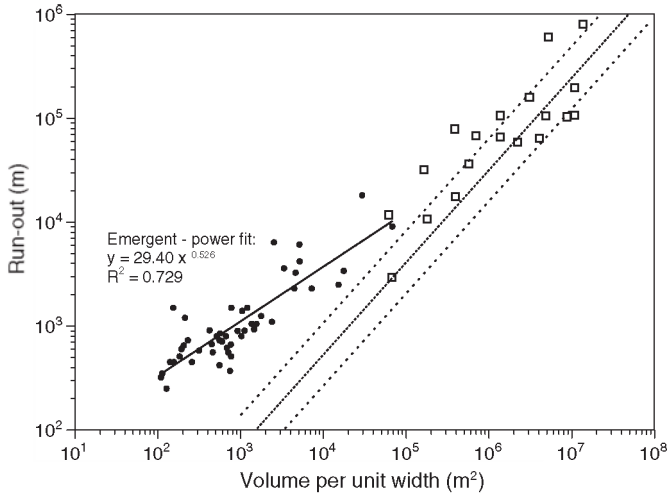

Fig. 12. Run-out distance versus volume per unit width for (emergent) sublacustrine landslides (black dots), and submarine landslides documented by Issler et al. (2005): COSTA project landslides (white squares) and Storegga debris flows (full line: power fit; dashed line: upper and lower bounds). Note that (emergent) sublacustrine landslides plot above the values for the Storegga debris flows. As the Storegga and COSTA databases essentially consist of emergent landslides, confined sublacustrine landslides are not plotted.

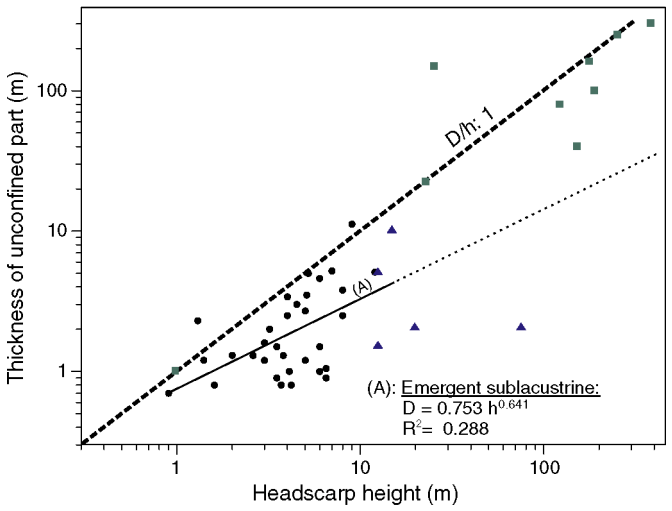

Fig. 14. Comparison of deposit thickness reduction in between (emergent) sublacustrine landslides (black dots), fjord landslides (blue triangles) and ocean margin landslides (green squares) (Hühnerbach et al., 2004). Ocean margin landslides plot above the power fit of sublacustrine and fjord landslides.

cohesive material may achieve long run-out distances on even very gentle slopes due to hydroplaning of the head of the flow, while sand-rich debris flows may evolve into a bipartite flow due to particle segregation. However, a wide range of compositions have been found in the sediment sequences involved in failure at ocean margins, fjords and lakes (Weaver et al., 2000; Cohen, 2003; Canals et al., 2004), and therefore initial sediment composition does not explain the general differences in mobility and disintegration found in between these three settings.

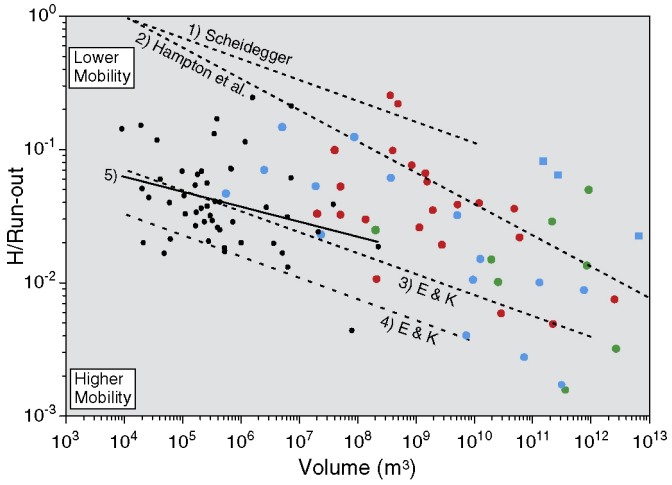

Fig. 13. Classical plot of run-out ratio versus volume for landslide mobility studies. Black circles: Frontally emergent sublacustrine landslides. Red and green circles: Western and Eastern Atlantic submarine landslides (Hühnerbach et al., 2004). Blue circles and blue squares correspond to respectively non-volcanic and volcanic submarine landslides derived from Hampton et al. (1996). 1) Average value for subaerial landslides proposed by Scheidegger (1973). 2) Upper bound for submarine landslides proposed by Hampton et al. (1996). 3 and 4) Lower bound values for submarine landslides and subaerial quick clay slides proposed by Edgers and Karlsrud (1982). Note that the power fit for sublacustrine landslides (5: full line) plots close to the lower boundary for submarine landslides (3) proposed by Edgers and Karlsrud (1982).

Landslides in fjords and lake basins take place on rather similar slope morphology. Both are characterized by relatively steep lateral or deltaic slopes and a abrupt slope break towards a nearly flat basin plain, indicated by their median slope angles for deposition and excavation areas (fjords: 0.625° and 5.5°; lakes: 0.4° and 6.1°). Submarine landslide catalogs showed a slightly negative correlation in between slope angle in the evacuation area and the run-out distance (McAdoo et al., 2000; Hühnerbach et al., 2004). Also, the abrupt slope reduction at the edge of the basin-plain should provoke a deceleration of dense flows originating upslope, causing enhanced deposition near the slope break (Mulder and Alexander, 2001b) and thus less material is available for achieving a long run-out distance. Therefore, the typical slope profile of lakes and fjords does not contribute to (or even hampers) their high landslide mobility.

In general, sedimentation rates in fjords and lakes (typically>1 mm/yr) are higher than at most ocean margins (Cohen, 2003) because of the direct sediment supply by inflowing river systems. Lacustrine and fjord sequences may therefore have a high water content and low consolidation values. The majority of cataloged sublacustrine landslides took place in lakes that are dominated by the deposition of diatom frustules (Lake Challa: Verschuren et al., 2009; Chilean lakes: Bertrand et al., 2008; Moernaut et al., 2009), which are renowned for their low degree of compaction (and thus high water content) during burial (Hamilton, 1976). As excavation depths in fjord and lacustrine landslides are relatively shallow (Table 1), the sediments involved in failure have a highly-unconsolidated nature. Contrarily, voluminous ocean margin landslides have a relatively deep excavation (McAdoo et al., 2000; Canals et al., 2004; Hühnerbach et al., 2004) and thus might consist of more consolidated sediments with larger shear strength. Thick ocean margin slope failures therefore require more energy to remold and transform (disintegrate) the initial sedimentary sequences and hence less potential energy can be transformed in kinetic energy, resulting in a relatively lower run-out and mobility.

It has to be noted that the discriminative patterns inferred in between landslides at ocean margins, fjords and lakes must be viewed from a general point. For example in some ocean margin landslide cases, very high landslide mobilities were found and were attributed to the highly-unconsolidated nature of the local source sediments, e.g. repeated failures in rapidly deposited glacial till at the Svalbard/Barents Sea margin (Dimakis et al., 2000; De Blasio et al., 2006).

8. Conclusions

By combining seismostratigraphic case studies with statistical analyses of morphometric parameters of sublacustrine landslides, this study has revealed valuable information regarding the frontal development and mobility of sublacustrine and submarine landslides:

1. Both frontally emergent and frontally confined landslides can take place on sublacustrine slopes, showing a continuous spectrum of frontal emplacement styles. Empirical data showed that the subsurface depth of the basal shear surface and the height drop (H^*) in between headscarp and frontal ramp are the main morphometric parameters determining the frontal emplacement style of landslides. These parameters essentially determine the height of the center of gravity of the failing mass with respect to the top of the frontal ramp, and correspond to the potential gravitational energy of the landslide versus the potential energy needed to ramp out of its stratigraphic position. The absolute values for these parameters are predominantly controlled by the slope profile (length, gradient, slope breaks) and geotechnical properties of the sedimentary sequence. This implies a predictive behavior for frontal emplacement style that is of key importance in the assessment of submarine landslide hazards, such as the development of tsunamis or destructive high-velocity sediment flows.
2. It is indispensable to separate frontally confined and emergent landslides in statistical morphometric studies, as their respective mechanisms of translation and emplacement are significantly different. Although sublacustrine landslides mostly have smaller dimensions than their submarine counterparts, comparable relationships between morphometric parameters were revealed, albeit with some significant exceptions. Obvious correlations emerged between volume-related parameters, while slope gradients show poor correlations with most other parameters. Several lines of evidence reveal that frontally emergent landslides in lakes (and fjords) generally exhibit a larger mobility and disintegration than expected by extrapolating the empirical relationships derived from ocean margin landslides. This could result from their shallower excavation, so that relatively less-consolidated sediments are involved in the mass-movement. Size distributions and the area/volume ratio of sublacustrine landslide deposits strongly deflect from the expected values, which is likely due to a strong morphological control (i.e., the confinement of lacustrine basins) on the size of slope failures and the resulting landslide deposits.

The lacustrine environment can be regarded as an easily accessible natural laboratory in which landslide processes are subjected to less lithological boundary conditions, but to more morphological control than landslides on ocean margins. Therefore, in some cases, systematic morphometric analysis can help to better understand subaqueous landslide processes in general, and the frontal development of landslides in particular.

Supplementary materials related to this article can be found online at doi:10.1016/j.margeo.2011.05.001.

Acknowledgments

The seismic data that were used in this study have been acquired by RCMG over the years by different field teams and in the context of different international partnerships and projects that were funded by different funding agencies. We wish to thank: F. Anselmetti, D. Ariztegui, F. Arnaud, C. Beck, D. Boone, R. Brümmer, E. Chapron, F. Charlet, H. Corbella, K. De Rycker, A. Duchkov, T. Haberzettl, K. Heirman, P. Huyghe, Y. Imbo, J. Klerkx, S. Kolobova, V. Matychenkov, L. Naudts, R. Pagni, A. Peña, A. Peretyatko, M. Pino, V. Romanovsky, W. San Martin, V.S. Seleznev, R. Urrutia, T. Van Cauwenberghe, M. Van Daele, P. Van Damme, D. Verschuren, W. Versteeg, B. Zolitschka and many others that were instrumental for the success of the seismic surveys; and the Belgian Science Policy Office, FWO-Vlaanderen, Special Research Fund (BOF) of the Universiteit Gent, EC Framework Programme 5, ESF (EuroCLIMATE Programme), INTAS, IPEV and the DFG for funding the field work. J. Moernaut was supported by the Institute for the Promotion of Innovation through Science and Technology in Flanders (IWT-Vlaanderen) and is currently funded by the Research Foundation — Flanders (FWO). We gratefully thank D. Masson, F. Anselmetti and an anonymous reviewer for their very detailed and constructive comments on an earlier version of this manuscript.

References

Bartetzko, A., Kopf, A.J., 2007. The relationship of undrained shear strength and porosity with depth in shallow (<50 m) marine sediments. Sedimentary Geology 196 (1–4), 235–249.
Bertrand, S., Charlet, F., Charlier, B., Renson, V., Fagel, N., 2008. Climate variability of southern Chile since the Last Glacial Maximum: a continuous sedimentological record from Lago Puyehue (40°S). Journal of Paleolimnology 39, 179–195.
Bull, S., Cartwright, J., Huuse, M., 2009. A review of kinematic indicators from mass-transport complexes using 3D seismic data. Marine and Petroleum Geology 26 (7), 1132–1151.
Callot, P., Odonne, F., Sempere, T., 2008. Liquification and soft-sediment deformation in a limestone megabreccia: the Ayabacas giant collapse, Cretaceous, southern Peru. Sedimentary Geology 212, 49–69.
Canals, M., Lastras, G., Urgeles, R., Casamor, J.L., Mienert, J., Cattaneo, A., De Batist, M., Haflidason, H., Imbo, Y., Laberg, J.S., Locat, J., Long, D., Longva, O., Masson, D.G., Sultan, N., Trincardi, F., Bryn, P., 2004. Slope failure dynamics and impacts from seafloor and shallow sub-seafloor geophysical data: case studies from the COSTA project. Marine Geology 213 (1–4), 9–72.
Chapron, E., 1999. Contrôles climatique et sismo-tectonique de la sedimentation lacustre dans l'Avant-Pays Alpin (lac du Bourget, Léman) Durant le Quaternaire recent. PhD Thesis, Université de Lille 1, 297 pp.
Chapron, E., Van Rensbergen, P., Beck, C., De Batist, M., Paillet, A., 1996. Lacustrine sedimentary records of brutal events in Lake Le Bourget (Northwestern Alps-Southern Jura). Quaternaire 7 (2–3), 155–168.
Chapron, E., Van Rensbergen, P., De Batist, M., Beck, C., Henriet, J.-P., 2004. Fluid-escape features as a precursor of a large sublacustrine sediment slide in Lake Le Bourget, NW Alps, France. Terra Nova 16, 305–311.
Chaytor, J.D., Ten Brink, U.S., Solow, A.R., Andrews, B.D., 2009. Size distribution of submarine landslides along the U.S. Atlantic Margin. Marine Geology 264, 16–27.
Cohen, A.S., 2003. Paleolimnology: The History and Evolution of Lake Systems. Oxford University Press. 500 pp.
Crusius, J., Anderson, R.F., 1995. Sediment focusing in six small lakes inferred from radionuclide profiles. Journal of Paleolimnology 13, 143–155.
Dan, G., Sultan, N., Savoye, B., Deverchere, J., Yelles, K., 2009. Quantifying the role of sandy-silty sediments in generating slope failures during earthquakes: example from the Algerian margin. International Journal of Earth Sciences 98, 769–789.
Davis, J.C., 1986. Statistics and Data Analysis in Geology (2nd edition). John Wiley & Sons, Inc., New York. 646 pp.
De Blasio, F.V., Elverhøi, A., Engvik, L.E., Issler, D., Gauer, P., Harbitz, C., 2006. Understanding the high mobility of subaqueous debris flows. Norwegian Journal of Geology 86, 275–284.
Dimakis, P., Elverhøi, A., Høeg, K., Solheim, A., Harbitz, C., Laberg, J.S., Vorren, T.O., Marr, J., 2000. Submarine slope stability on high-latitude glaciated Svalbard–Barents Sea margin. Marine Geology 162, 303–316.
Dussauge, C., Grasso, J.R., Helmstetter, A.S., 2003. Statistical analysis of rockfall volume distributions: implications for rockfall dynamics. Journal of Geophysical Research-Solid Earth 108 (B6), 2286. doi:10.1029/2001JB000650.
Edgers, L., Karlsrud, K., 1982. Soil Flows Generated by Submarine Flows: Case Studies and Consequences. NGI Publication 143. Norges Geotekniske Institutt, Oslo, Norway.
Elverhøi, A., Breien, H., De Blasio, F.V., Harbitz, C.B., Pagliardi, M., 2010. Submarine landslides and the importance of the initial sediment composition for run-out length and final deposit. Ocean Dynamics 60, 1027–1046.
Finckh, P., Kelts, K., Lambert, A., 1984. Seismic stratigraphy and bedrock forms in perialpine lakes. Geological Society of America Bulletin 95, 1118–1128.
Frey-Martinez, J., Cartwright, J., Hall, B., 2005. 3D seismic interpretation of slump complexes: examples from the continental margin of Israel. Basin Research 17 (1), 83–108.
Frey-Martinez, J., Cartwright, J., James, D., 2006. Frontally confined versus frontally emergent submarine landslides: a 3D seismic characterization. Marine and Petroleum Geology 23 (5), 585–604.
Gafeira, J., Bulat, J., Evans, D., 2007. The southern flank of the Storegga Slide: imaging and geomorphological analyses using 3D seismic. In: Lykousis, V., Sakellariou, D., Locat, J. (Eds.), Submarine Mass Movements and Their Consequences. Springer Netherlands, pp. 57–65.
Gamberi, F., Rovere, M., Marani, M., 2011. Mass-transport complex evolution in a tectonically active margin (Gioia Basin, Southeastern Tyrrhenian Sea). Marine Geology 279 (1–4), 98–110.

Gee, M.J.R., Gawthorpe, R.L., Friedmann, J.S., 2005. Giant striations at the base of a submarine landslide. Marine Geology 214 (1–3), 287–294.
Green, A., Uken, R., 2008. Submarine landsliding and canyon evolution on the northern KwaZulu-Natal continental shelf, South Africa, SW Indian Ocean. Marine Geology 254 (3–4), 152–170.
Haflidason, H., Lien, R., Sejrup, H.P., Forsberg, C.F., Bryn, P., 2005. The dating and morphometry of the Storegga Slide. Marine and Petroleum Geology 22 (1–2), 123–136.
Håkanson, L., Jansson, M., 2002. Principles of Lake Sedimentology (2nd edition). The Blackburn Press, New Jersey. 316 pp.
Hamilton, E.L., 1976. Variations of density and porosity with depth in deep-sea sediments. Journal of Sedimentary Petrology 46 (2), 280–300.
Hampton, M.A., Lee, H.J., Locat, J., 1996. Submarine landslides. Reviews of Geophysics 34 (1), 33–59.
Harbitz, C.B., Løvholt, F., Pedersen, G., Masson, D.G., 2006. Mechanisms of tsunami generation by submarine landslides: a short review. Norwegian Journal of Geology 86, 255–264.
Harders, R., Kutterolf, S., Hensen, C., 2010. Tephra layers: a controlling factor on submarine translational sliding? Geochemistry Geophysics Geosystems 11 (5). doi:10.1029/2009GC002844.
Hühnerbach, V., Masson, D.G., partners of the COSTA project, 2004. Landslides in the North Atlantic and its adjacent seas: an analysis of their morphology, setting and behaviour. Marine Geology 213 (1–4), 343–362.
Huvenne, V.A.I., Croker, P.F., Henriet, J.-P., 2002. A refreshing 3D view of an ancient sediment collapse and slope failure. Terra Nova 14 (1), 33–40.
Issler, D., De Blasio, F.V., Elverhoi, A., Bryn, P., Lien, R., 2005. Scaling behaviour of clay-rich submarine debris flows. Marine and Petroleum Geology 22 (1–2), 187–194.
Karlin, R.E., Holmes, M., Abella, S.E.B., Sylwester, R., 2004. Holocene landslides and a 3500-year record of Pacific Northwest earthquakes from sediments in Lake Washington. Geological Society of America Bulletin 116 (1–2), 94–108.
Lawrence, G.W.M., Cartwright, J.A., 2009. The initiation of sliding on the mid Norway margin of the Møre Basin. Marine Geology 259, 21–35.
Ledoux, G., Lajeunesse, P., Chapron, E., St-Onge, G., 2010. Multibeam bathymetry investigations of mass-movements in Lake Le Bourget (NW Alps, France) using a portable platform. In: Mosher, D.C., et al. (Ed.), Submarine Mass Movements and Their Consequences. : Advances in Natural and Technological Hazards Research, 28. Springer Netherlands, pp. 423–434.
Legros, F., 2002. The mobility of long-runout landslides. Engineering Geology 63, 301–331.
Leynaud, D., Sultan, N., Mienert, J., 2007. The role of sedimentation rate and permeability in the slope stability of the formerly glaciated Norwegian continental margin: the Storegga Slide model. Landslides 4 (4), 297–309.
Locat, J., Lee, H.J., 2002. Submarine landslides: advances and challenges. Canadian Geotechnical Journal 39 (1), 193–212.
Mandl, G., Crans, W., 1981. Gravitational gliding in deltas. Special Publication Geological Society of London 9, 41–54.
Masson, D.G., Harbitz, C.B., Wynn, R.B., Pedersen, G., Løvholt, F., 2006. Submarine landslides: processes, triggers and hazard prediction. Philosophical Transactions of the Royal Society A 364, 2009–2039. doi:10.1098/rsta.2006.1810.
McAdoo, B.G., Pratson, L.F., Orange, D.L., 2000. Submarine landslide geomorphology, US continental slope. Marine Geology 169 (1–2), 103–136.
Micallef, A., Berndt, C., Masson, D.G., Stow, D.A.V., 2007. Fractal statistics of the Storegga Slide. In: Lykousis, V., Sakellariou, D., Locat, J. (Eds.), Submarine Mass Movements and Their Consequences. Springer Netherlands, pp. 3–10.
Micallef, A., Berndt, C., Masson, D.G., Stow, D.A.V., 2008. Scale invariant characteristics of the Storegga Slide and implications for large-scale submarine mass movements. Marine Geology 247 (1–2), 46–60.
Moernaut, J., De Batist, M., Charlet, F., Heirman, K., Chapron, E., Pino, M., Brummer, R., Urrutia, R., 2007. Giant earthquakes in South-Central Chile revealed by Holocene mass-wasting events in Lake Puyehue. Sedimentary Geology 195 (3–4), 239–256.
Moernaut, J., De Batist, M., Heirman, K., Van Daele, M., Pino, M., Brummer, R., Urrutia, R., 2009. Fluidization of buried mass-wasting deposits in lake sediments and its relevance for paleoseismology: results from a reflection seismic study of lakes Villarrica and Calafquén (South-Central Chile). Sedimentary Geology 213 (3–4), 121–135.
Moernaut, J., Verschuren, D., Charlet, F., Kristen, I., Fagot, M., De Batist, M., 2010. The seismic-stratigraphic record of lake-level fluctuations in Lake Challa: hydrological stability and change in equatorial East Africa over the last 140 kyr. Earth and Planetary Science Letters 290 (1–2), 214–223.
Mulder, T., Alexander, J., 2001a. The physical character of subaqueous sedimentary density flows and their deposits. Sedimentology 48 (2), 269–299.
Mulder, T., Alexander, J., 2001b. Abrupt change in slope causes variation in the deposit thickness of concentrated particle-driven density currents. Marine Geology 175 (1–4), 221–235.
Mulder, T., Cochonat, P., 1996. Classification of offshore mass movements. Journal of Sedimentary Research 66, 43–57.
Nardin, T.R., Hein, F.J., Gorsline, D.S., Edwards, B.D., 1979. A review of mass movement processes, sediment and acoustical characteristics, and contrasts in slope and base of slope systems versus canyon fed basin floor systems. In: Doyle, L.J., Pilkey, O.H. (Eds.), Geology of Continental Slopes: Society of Economic Paleontologists and Mineralogists Special Publications, 27, pp. 61–73.
Normark, W.R., McGann, M., Sliter, R., 2004. Ages of Palos Verdes submarine debris avalanche, southern California. Marine Geology 203 (3–4), 247–259.
Piper, D.J.W., Shor, A.N., Hughes-Clarke, J.E., 1988. The 1929 Grand Banks earthquake, slump and turbidity current. In: Clifton, H.E. (Ed.), Sedimentologic Consequences of Convulsive Geologic Events: Special Paper Geological Society of America, 229, pp. 77–92.
Scheidegger, A.E., 1973. On the prediction of the reach and velocity of catastrophic landslides. Rock Mechanics and Rock Engineering 5, 231–236.
Schnellmann, M., Anselmetti, F.S., Giardini, D., McKenzie, J.A., Ward, S.N., 2002. Prehistoric earthquake history revealed by lacustrine slump deposits. Geology 30 (12), 1131–1134.
Schnellmann, M., Anselmetti, F.S., Giardini, D., McKenzie, J.A., 2005. Mass movement-induced fold-and-thrust belt structures in unconsolidated sediments in Lake Lucerne (Switzerland). Sedimentology 52 (2), 271–289.
Schnellmann, M., Anselmetti, F.S., Giardini, D., McKenzie, J.A., 2006. 15,000 years of mass-movement history in Lake Lucerne: implications for seismic and tsunami hazards. Eclogae Geologicae Helvetiae 99 (3), 409–428.
Scholz, C.A., Karp, T., Brooks, K.M., Milkereit, B., Amoako, P.Y.O., Arko, J.A., 2002. Pronounced central uplift identified in the Bosumtwi impact structure, Ghana, using multichannel seismic reflection data. Geology 30 (10), 939–942.
Solheim, A., Berg, K., Forsberg, C.F., Bryn, P., 2005. The Storegga Slide complex: repetitive large scale sliding with similar cause and development. Marine and Petroleum Geology 22 (1–2), 97–107.
Strachan, L., 2002. Geometry to genesis: a comparative field study of submarine slump deposits and their modes of formation. PhD thesis, Cardiff and Imperial College (UK). 412 pp.
Strasser, M., Anselmetti, F.S., Fah, D., Giardini, D., Schnellmann, M., 2006. Magnitudes and source areas of large prehistoric northern Alpine earthquakes revealed by slope failures in lakes. Geology 34 (12), 1005–1008.
Strasser, M., Stegmann, S., Bussmann, F., Anselmetti, F.S., Rick, B., Kopf, A., 2007. Quantifying subaqueous slope stability during seismic shaking: Lake Lucerne as model for ocean margins. Marine Geology 240 (1–4), 77–97.
ten Brink, U.S., Geist, E.L., Andrews, B.D., 2006. Size distribution of submarine landslides and its implication to tsunami hazard in Puerto Rico. Geophysical Research Letters 33, L11307. doi:10.1029/2006GL026125.
ten Brink, U.S., Barkan, R., Andrews, B.D., Chaytor, J.D., 2009. Size distributions and failure initiation of submarine and subaerial landslides. Earth and Planetary Science Letters 287, 31–42.
Trincardi, F., Argnani, A., 1990. Gela submarine slide — a major basin-wide event in the Plio-Quaternary foredeep of Sicily. Geo-Marine Letters 10 (1), 13–21.
Tripsanas, E.K., Piper, D.J.W., Jenner, K.A., Bryant, W.R., 2008. Submarine mass-transport facies: new perspectives on flow processes from cores on the eastern North American margin. Sedimentology 55 (1), 97–136.
Van Rensbergen, P., De Batist, M., Beck, C., Chapron, E., 1999. High-resolution seismic stratigraphy of glacial to interglacial fill of a deep glacigenic lake: Lake Le Bourget, Northwestern Alps, France. Sedimentary Geology 128, 99–129.
Verschuren, D., Sinninghe Damsté, J.S., Moernaut, J., Kristen, I., Blaauw, M., Fagot, M., Haug, G.H., CHALLACEA project members, 2009. Half-precessional dynamics of monsoon rainfall near the East African equator. Nature 462, 637–641.
Waldmann, N., Ariztegui, D., Anselmetti, F.S., Austin, J.A., Dunbar, R., Moy, C.M., Recasens, C., 2008. Seismic stratigraphy of Lago Fagnano sediments (Tierra del Fuego, Argentina) — a potential archive of paleoclimatic change and tectonic activity since the Late Glacial. Geologica Acta 6 (1), 101–110.
Weaver, P.P.E., Wynn, R.B., Kenyon, N.H., Evans, J., 2000. Continental margin sedimentation, with special reference to the north-east Atlantic margin. Sedimentology 47 (1), 239–256.